J Solid State Electrochem (2001) 5: 160–187
DOI 10.1007/s100080000141

REVIEW

Vladislav V. Kharton · Evgeny N. Naumovich
Aleksey A. Yaremchenko · Fernando M.B. Marques

Research on the electrochemistry of oxygen ion conductors in the former Soviet Union

IV. Bismuth oxide-based ceramics

Received: 22 March 2000 / Accepted: 19 April 2000 / Published online: 3 March 2001

Abstract Following previous reviews of research results on oxygen ion-conducting materials obtained in the former USSR, this article addresses the case of Bi_2O_3-based compositions. Phase formation in oxide systems with Bi_2O_3, thermal expansion, stability, bulk transport properties and oxygen exchange of bismuth oxide solid electrolytes are briefly discussed. Primary attention is focused on oxides with high ionic and mixed conductivity, including stabilized fluorite-type (δ) and sillenite (γ) phases of Bi_2O_3, γ-$Bi_4V_2O_{11}$ and other compounds of the aurivillius series. Another major point being addressed is on the applicability of these materials in high-temperature electrochemical cells, which is limited by numerous specific disadvantages of Bi_2O_3-based ceramics. The electrochemical properties of various electrode systems with bismuth oxide electrolytes are also briefly analyzed.

Key words Bismuth oxide · Solid electrolyte · Mixed conductor · Ionic conductivity · Electronic transport

Introduction

Oxide solid electrolytes and mixed ionic-electronic conductors are of great interest for numerous technological applications such as sensors of various types, solid oxide fuel cells (SOFCs), electrolyzers, and ceramic membranes for high-purity oxygen separation and partial oxidation of hydrocarbons. Among oxygen ion-conducting materials, oxide phases derived from Bi_2O_3 deserve special emphasis owing to their high ionic conductivity with respect to other well-known solid electrolytes. Examples of such phases are stabilized δ-Bi_2O_3, having a fluorite-type structure with a very high level of deficiency in the oxygen sublattice, and γ-$Bi_4V_2O_{11}$ (the so-called BIMEVOX series), which belongs to the aurivillius series. At the same time, Bi_2O_3-based materials possess a number of specific disadvantages, including excessively high thermal expansion coefficients (TECs), thermodynamic instability in reducing atmospheres, volatilization of bismuth oxide at moderate temperatures, a high corrosion activity and low mechanical strength. Owing to this, the applicability of these oxides in electrochemical cells is considerably limited.

This paper is part IV of our review aiming to improve the access of Western scientists to the research results in the field of oxygen ionic conductors obtained in the former USSR. Since most of these results were published in Russian, they are still poorly known in other countries. Three previous parts were focused on zirconia-based ceramics [1], perovskite-like oxides [2] and materials based on CeO_2, ThO_2 and HfO_2 [3]. The present work is devoted to Bi_2O_3-based phases, which are only of moderate practical importance owing to the above-listed disadvantages, but are important from a viewpoint of fundamental knowledge and as a potential basis for further development of novel materials.

As for the previous reviews, most attention is given here to the results considered of interest for the state-of-the-art electrochemistry of oxygen ionic conductors. Other work is only briefly listed in order to provide references for researchers interested in such information. In particular, only few references on Bi_2O_3-containing electroceramics, high-temperature superconductors, optical materials and protective coatings are included. Furthermore, no attempt is made to compare the results obtained in Soviet and Western scientific centers. As any reader familiar with the subject might conclude from this

V.V. Kharton (✉)[1] · E.N. Naumovich · A.A. Yaremchenko
Institute of Physicochemical Problems,
Belarus State University, 14 Leningradskaya Str.,
220080 Minsk, Republic of Belarus
E-mail: kharton@cv.ua.pt
Tel.: +351-234-370263
Fax: +351-234-425300

F.M.B. Marques
Department of Ceramics and Glass Engineering,
UIMC, University of Aveiro, 3810-193 Aveiro, Portugal

Present address:
[1]Department of Ceramics and Glass Engineering,
UIMC, University of Aveiro, 3810-193 Aveiro, Portugal

paper, such comparison would obviously show enormous coherence between all the research results. This may be illustrated, for example, by the similarity of recent reviews on Bi_2O_3-based solid electrolytes [4, 5, 6, 7]. References to papers published in international journals included in this work were mainly selected to demonstrate the most important relationships between experimental data sets.

This review consists of nine main sections. The first of them is devoted to physicochemical and transport properties of pure bismuth oxide. The next seven sections analyze information available on various phases formed by Bi_2O_3 and other metal oxides; primary emphasis is given to materials tested from the viewpoint of high-temperature electrochemistry, including determination of partial ionic and electronic conductivities. The last section considers the results of application tests and electrochemical properties of Bi_2O_3-based ionic conductors, such as oxygen exchange, polarization of various electrodes in contact with bismuth oxide electrolytes, and response of potentiometric oxygen sensors based on these materials.

One should mention that a brief analysis as well as selected data on physicochemical and electrochemical properties of Bi_2O_3-based solid electrolytes and mixed conductors can be found in a number of books [8, 9, 10, 11] and reviews [4, 5]. Numerous phase diagrams of oxide systems containing bismuth oxide have been collected and analyzed [12, 13].

Bismuth oxide phases and their transport properties

Phase relationships in the Bi-O system

A number of different compounds exist in the binary Bi-O system, where the oxidation state of bismuth varies from $+2$ to $+5$. In a simplified description, these compounds may be considered as BiO, Bi_2O_3, Bi_2O_4 and Bi_2O_5 [14]; several polymorph modifications are found for BiO and Bi_2O_3. However, detailed electron diffraction studies demonstrated the existence of at least five BiO_x separate phases in the range $x = 1$–1.5 [15]. As a rule, since reduction-oxidation processes in the Bi-O system are relatively easy (see, for example, [15, 16]), high concentrations of specific charged defects are typical for all bismuth oxide compounds; this may lead to formation of various ordered structures. The oxidized phases, where the average oxidation state of bismuth is significantly higher than $3+$, are thermodynamically unstable under usual conditions. For example, the formation enthalpy of Bi_2O_5 is approximately equal to -185 kJ/mol, which is significantly less than the corresponding values for As_2O_5 and Sb_2O_5, in agreement with the instability of the pentavalent bismuth oxide phase [17]. Owing to experimental difficulties in the determination of the exact oxidation state of bismuth in the oxide phases, namely volatilization, high corrosion activity and the low melting point of metallic Bi, the compound stable in atmospheric air is often assumed to be bismuth(III) oxide, Bi_2O_3 [4, 5, 18]. This assumption will be maintained in all cases where separate determination of the oxidation state of bismuth cations or oxygen content was not performed.

Bismuth(III) oxide forms two thermodynamically stable polymorph modifications, namely the monoclinic α-phase and the fcc δ-phase [18, 19]. The $\alpha \rightarrow \delta$ transition occurs at 978–1013 K [18]; the variation of the transition temperature in such a wide range is related to the purity of samples (Table 1), their thermal pre-history [18] and oxygen stoichiometry [19]. For sufficiently pure bismuth oxide, the $\alpha \rightarrow \delta$ transition takes place at 996–1003 K [18, 19, 20]. Cooling down of the high-temperature δ-phase is accompanied by a large hysteresis, when formation of an intermediate metastable tetragonal β-phase and a bcc γ-polymorph (sillenite phase) may occur [18, 19]. The metastability of the β- and γ-phases is determined by an excessive length of the metal-metal distances in the lattice, since the chemical bonds in bismuth oxide compounds are formed not only between O and Bi ions, but also between bismuth pairs [15, 21]. Therefore, appropriate doping may lead to shorter Bi-Bi distances, stabilizing these phases down to lower temperatures [21]. Analogously, the temperatures of the phase transition in bismuth oxide depend on the oxygen partial pressure [19], which affects the oxygen content and, thus, interatomic distances.

Detailed electron diffraction studies of bismuth oxide films with variable oxygen content [14, 15, 22, 23, 24, 25] showed possible oxygen nonstoichiometry of the phases

Table 1 Thermodynamic data for phase transitions of Bi_2O_3

Purity	Atmosphere	Process	Transition	Temperature (K)	Enthalpy (kJ mol^{-1})	Ref.
≥99%	Air	Heating	$\alpha \rightarrow \delta$	1000	63.4	[18]
		Cooling	$\delta \rightarrow \alpha$	923	60.0	
≥99.5%	Air	Heating	$\alpha \rightarrow \delta$	998	72.1	[18]
		Cooling	$\delta \rightarrow \beta$	945	58.1	
			$\beta \rightarrow \alpha$	880	23.7	
≥99.99%	Air	Heating	$\alpha \rightarrow \delta$	996	89.2	[18]
		Cooling	$\delta \rightarrow \beta$	940	67.3	
			$\beta \rightarrow \alpha$	889	28.1	
99.97%	O_2	Heating	$\alpha \rightarrow \delta$	1003	–	[19]
	Air			1000	78.3	
	CO_2			1000	–	
	Ar			998	–	

present in air. This conclusion is supported by data [19] demonstrating that the low-temperature stability limits of the β- and δ-phases are displaced towards lower temperatures with reducing oxygen partial pressure, when the oxygen content in the oxides decreases. The bismuth oxide δ-phase [22] was identified as Bi_2O_{3-x} ($x \leq 0.3$); the structure [22] was found to be in agreement with the model proposed by Sillen [26]. The composition $Bi_2O_{2.5}$ was ascribed to the tetragonal β-phase [15, 23]. Note that, neglecting the simple relationship between unit cell parameters of the β- and δ-phases ($a\beta \approx a\delta/\sqrt{2}$; $c\beta \approx a\delta$), this tetragonal structure cannot be considered as a two-dimensional ordered superlattice of the fluorite-like cubic δ-phase [15]. A rhombohedrally distorted sphalerite-type [24] and a cubic [27] modification were reported for the BiO compound which is, in contrast to other Bi-O phases, stoichiometric. A summary of the bismuth oxide phases detected by electron diffraction is given in Table 2. It should be mentioned that the data [14, 15, 22, 23, 24, 25] obtained using thin-film samples may differ from bulk properties of corresponding phases as a result, in particular, of an effect of the substrate on the film properties. As an example, the maximum oxygen content in Bi_2O_x, obtained for thin films, was as low as $x = 2.7$–2.8 [15]. A probable influence of the thin-film form of the sample on the phase composition has been noted [28].

Conductivity of Bi_2O_3 phases

Systematic data on electrical conductivity, Seebeck coefficients and oxygen ion transference numbers of Bi_2O_3 have been reported [18, 29, 30, 31]. Significant activity was devoted to the electrical and electrochemical properties of bismuth oxide films (for example, [28, 32, 33, 34]). According to these results, the α-phase is a predominantly electronic conductor [30]; the ion transference numbers of the monoclinic modification of bismuth oxide are negligible [18, 29, 30]. The electronic conductivity of this phase depends significantly on impurity content and oxidation state of bismuth and may be affected by the presence of water vapor in the atmosphere [18, 30]. As an example, repeated heating-cooling cycles lead to a considerable increase in the conductivity of α-Bi_2O_3 owing to interaction of the samples with the electrodes, including platinum and gold [18]. Annealing of Bi_2O_3 in a CO atmosphere even at temperatures as low as 550 K results in the formation of metallic bismuth, which increases the total conductivity by 10–15 times [30].

Transition from the α- to the fluorite-like δ-phase occurs with a dramatic increase in the oxygen ionic conductivity; the ion transference numbers become close to unity (Figs. 1 and 2). The temperature dependencies of the total conductivity around the transition can be approximated as [29]:

$$\text{at } 673 - 893 \text{ K } \ln(\sigma \times T) = (8.5 \pm 0.3) - (61.4 \pm 2.1)/RT \quad (1)$$

$$\text{at } 953 - 1053 \text{ K } \ln(\sigma \times T) = (12.33 \pm 0.08) - (40.2 \pm 0.6)/RT \quad (2)$$

with $\sigma \times T$ expressed in S cm^{-1} K and the activation energies expressed in kJ mol^{-1}. Poluyan [18] reported similar values for the activation energy (63 ± 3 kJ mol^{-1}

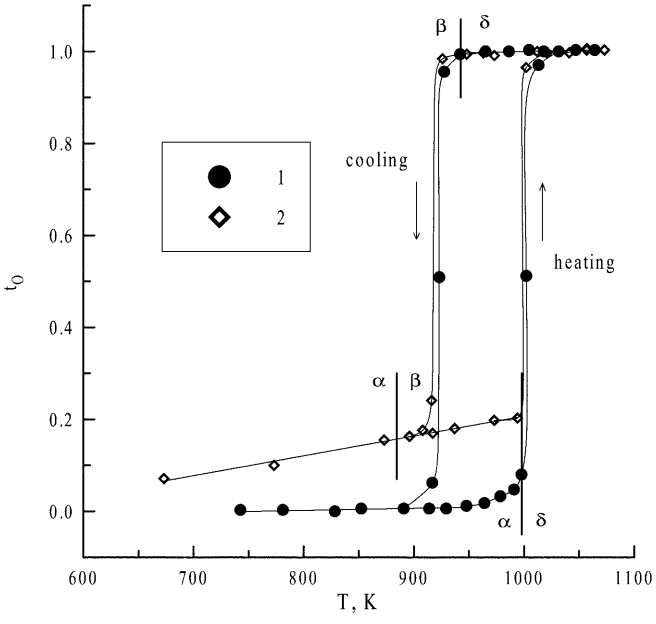

Fig. 1 Temperature dependence of the oxygen ion transference numbers of bismuth(III) oxide measured by the e.m.f. method (oxygen pressure gradient, 1.0/0.21 atm): *1*, data from [18]; *2*, data from [29]. The phase transitions are marked using the results from [18]

Table 2 Crystal structure data for bismuth oxide phases

Phase	Symmetry, space group	Lattice parameters	Number of formula units, Z	Ref.
BiO	Rhombohedral, C_{3v}^5–$R3m$	$a = 0.394$ nm, $\alpha = 59°$	3	[24]
$Bi_2O_{2.7-2.8}$	Tetragonal, D_{4h}^{17}–$I4/mmm$	$a = 0.385$ nm, $c = 1.225$ nm	2	[14]
$Bi_2O_{2.3-2.4}$	Tetragonal, D_{4h}^{17}–$I4/mmm$	$a = 0.385$ nm, $c = 3.510$ nm	6	[25]
β-$Bi_2O_{2.5}$	Tetragonal, D_{2d}^4–$P\bar{4}2_1c$	$a = 0.775$ nm, $c = 0.563$ nm	4	[23]
δ-Bi_2O_{3-x}	Cubic, O_h^4–$Pn3m$	$a = 0.545$ nm	2	[22]

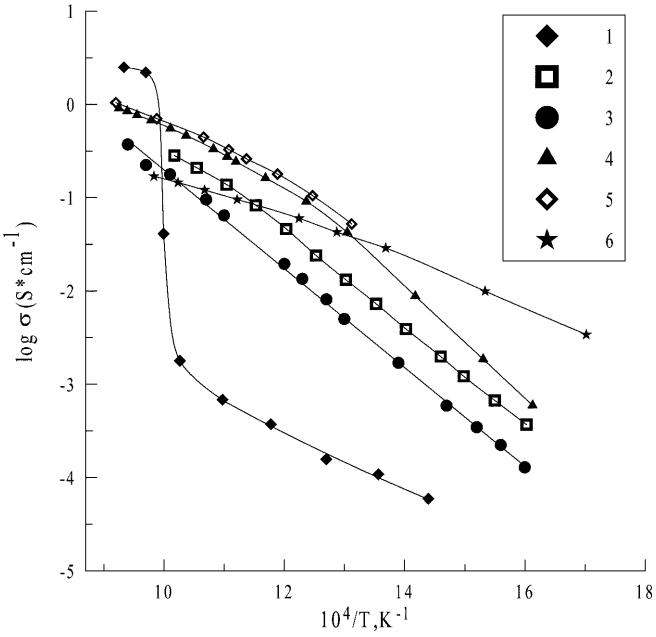

Fig. 2 Temperature dependence of the total electrical conductivity in air: *1*, Bi_2O_3 (99.99%) [18]; *2*, $(Bi_2O_3)_{0.77}(Y_2O_3)_{0.23}$ [18]; *3*, $(Bi_{0.75}Y_{0.25}O_{1.5})_{0.95}(PrO_{1.83})_{0.05}$ [45]; *4*, $(Bi_{0.95}Zr_{0.05})_{0.85}Y_{0.15}O_{1.5+\delta}$ [41]; *5*, $Bi_{0.92}Nb_{0.08}O_{1.5+\delta}$ [40]; *6*, $Bi_2V_{0.9}Cu_{0.1}O_{5.5-\delta}$ [48]

for the α- and 38 ± 2 kJ mol^{-1} for the δ-phase). Data on the electrical conductivity and Seebeck coefficients of bismuth oxide in the course of melting of the δ-phase provide no definite information on possible changes in the conductivity mechanisms [31].

On cooling, the ionic conductivity behavior is similar to the heating regime, excluding the thermal hysteresis due to formation of a metastable phase (Fig. 1). The conductivity of the β-phase is mixed ionic-electronic; the transition to the α-modification decreases the ionic transport to zero.

Reduction and thermal expansion of bismuth oxide

According to the results of Poluyan [18], the equilibrium oxygen pressure over bismuth oxide studied using the cell:

$$W,\ Bi - Bi_2O_3|ZrO_2 + Y_2O_3|O_2(0.21\ atm), Pt \qquad (3)$$

can be approximated in the temperature range 860–1073 K by the equation:

$$\log p(O_2) = -(19600 \pm 200)/T + (14.2 \pm 0.2) \qquad (4)$$

with $p(O_2)$ expressed in Pa. These values are significantly higher than the zirconium dioxide dissociation oxygen pressure, showing a weaker stability of Bi_2O_3 with respect to zirconia-based electrolytes. A similar conclusion may be obtained from the values of the Bi_2O_3 decomposition potential in melted NaOH, which is as low as 0.4 V at 723 K [16].

Table 3 Thermal expansion coefficients for Bi_2O_3-based ceramics

Composition	Average TEC values		Ref.
	Temperature range (K)	$\bar{\alpha} \times 10^{-6}$ (K^{-1})	
Bi_2O_3 (99%)	400–800/940–1020	12.9/20.0	[36]
Bi_2O_3 (99.99%)	400–900/940–1025	10.6/20.2	[18]
	930–840 (cooling)	19.2	
$Bi_{0.95}Co_{0.05}O_{1.5}$	300–940	16.1	[37]
$(Bi_{0.70}Co_{0.30})_{0.90}Y_{0.10}O_{1.5}$	400–650/650–1000	14.0/20.9	[38]
$(Bi_2O_3)_{0.8}(Er_2O_3)_{0.2}$	400–1090	17.2	[36]
	598–998	19	[39]
$Bi_{0.92}Nb_{0.08}O_{1.5+\delta}$	300–700/700–1020	12.6/26	[40]
$Bi_{0.90}Nb_{0.10}O_{1.5+\delta}$	300–680/680–1040	10.7/20.6	[40]
$Bi_{0.84}Nb_{0.16}O_{1.5+\delta}$	300–700/700–1040	10.3/17.5	[40]
$(Bi_{0.95}Nb_{0.05})_{0.90}Ho_{0.10}O_{1.5+\delta}$	340–690/690–1030	13.3/24	[41]
$(Bi_{0.95}Nb_{0.05})_{0.85}Ho_{0.15}O_{1.5+\delta}$	330–690/690–1050	13.1/20.4	[41]
$(Bi_{0.92}Nb_{0.08})_{0.90}Ho_{0.10}O_{1.5+\delta}$	340–710/710–1010	12.8/21.1	[41]
$(Bi_{0.90}Pb_{0.10})_{0.80}Y_{0.20}O_{1.5}$	300–540/680–970	10.4/21.2	[42]
$(Bi_{0.68}Pb_{0.32})_{0.85}Y_{0.15}O_{1.5}$	300–620/660–820	12.6/22.6	[43]
$(Bi_{0.68}Pb_{0.32})_{0.80}Y_{0.20}O_{1.5}$	300–650/690–890	11.3/21.8	[43]
$(Bi_2O_3)_{0.75}(Y_2O_3)_{0.25}$	400–1090	14.6	[36]
	598–998	14.3	[39]
	400–540/540–710/710–1025	10.7/15.0/19.8	[18]
$(Bi_2O_3)_{0.67}(Y_2O_3)_{0.33}$	400–1090	16.8	[36]
$(Bi_{0.75}Y_{0.25}O_{1.5})_{0.90}(PrO_{1.833})_{0.10}$	450–800/800–950	14.4/20.5	[44]
$(Bi_{0.75}Y_{0.25}O_{1.5})_{0.85}(PrO_{1.833})_{0.15}$	400–800/800–950	12.5/20.5	[44]
$(Bi_{0.70}Y_{0.30}O_{1.5})_{0.90}(PrO_{1.833})_{0.10}$	400–700/700–950	9.74/16.1	[45]
$(Bi_{0.70}Y_{0.30}O_{1.5})_{0.85}(PrO_{1.833})_{0.15}$	500–750/750–950	10.0/15.5	[45]
$(Bi_{0.95}Zr_{0.05}O_{1.525})_{0.85}(YO_{1.5})_{0.15}$	340–900/900–970	12.31/20.11	[46, 47]
$(Bi_{0.95}Zr_{0.05}O_{1.525})_{0.80}(YO_{1.5})_{0.20}$	340–900/900–970	13.36/19.28	[46, 47]
$(Bi_{0.90}Zr_{0.10}O_{1.55})_{0.85}(YO_{1.5})_{0.15}$	340–900/900–970	14.38/19.19	[46, 47]
$Bi_2V_{0.90}Cu_{0.10}O_{5.5-\delta}$	300–730/730–1030	15.3/18.0	[48]
$Bi_{1.90}La_{0.10}V_{0.90}Cu_{0.10}O_{5.5-\delta}$	300–640/640–1000	15.0/17.7	[48]
$BaBiO_{3-\delta}$	400–670/670–875	13.5/19.3	[18]
$Bi_2CuO_{4\pm\delta}$	300–800/850–1000	5–6/10–11	[49]

In contrast to zirconia-based ceramics [1], TECs of the ionically conductive phases of bismuth oxide are relatively high (Table 3). For example, average TEC values for the β- and δ-polymorphs are 19.2×10^{-6} and 20.2×10^{-6} K^{-1}, respectively [18]. This behavior is in agreement with the phenomenological theory of ionic transport [35], which showed that a high mobility of ions correlates with a high thermal expansion. TECs of bismuth oxide depend, as would be expected, on impurity content. For the α-phase, increasing impurity content leads to an increase in thermal expansion, whereas the behavior of the δ-phase is the opposite [18].

Phase transitions in the course of heating-cooling cycles lead to sharp volume changes of sintered Bi_2O_3 ceramics [18]. For the transitions $\alpha \rightarrow \delta$, $\delta \rightarrow \beta$ and $\beta \rightarrow \alpha$, the changes in volume were 6.7, 2.0 and 3.8%, respectively [18].

Fluorite-type solid electrolytes in the systems Bi_2O_3-Ln_2O_3 (Ln=Y, La, Sm, Dy, Ho, Er)

Phase relationships and stability

After the pioneering work of Takahashi et al. (in particular, [52]), claiming stabilization down to room temperature of the high-conductive δ-phase by addition of rare-earth elements (REE), numerous research projects were focused on phase composition, structure and thermodynamic stability of oxide compounds in the systems Bi_2O_3-Ln_2O_3 (Ln = REE or Y). In these systems, a stabilization of the δ-phase down to temperatures significantly lower than the $\alpha \rightarrow \delta$ transition temperature was found for dopants such as Y [18, 39, 47, 51, 53, 54, 55], Dy [51] and Er [39, 50, 51]. However, recent studies [56, 57, 58] showed a metastability of the fcc solid solutions in the binary oxide systems at temperatures below 770–870 K, which leads to the decomposition of the fluorite-like phase with time. Similar results were also obtained for ternary oxide systems [40, 41, 59]. Thermodynamic results on the Bi_2O_3-Y_2O_3 system [55] confirm partly the conclusion on the metastability of the δ-phase at low temperature, at least for compositions containing more than 37 mol% of yttrium oxide. Along with phase instability, another reason for disagreement in the literature on existing phases is the strong dependence of the phase composition on the thermal pre-history of the samples [18]. For example, stabilization of the δ-phase in Bi_2O_3-Y_2O_3 ceramics, after annealing and slow cooling in air, was reported to be in the concentration range 23–40 mol%, while quenching enlarges these limits up to 10–50 mol% of yttria [18].

Results of thermodynamic studies on selected δ-Bi_2O_3-based materials, including the low oxygen-pressure decomposition limits and the free energy of formation, have been reported [18, 50, 51, 54, 55]. A summary of the stability limits at low oxygen partial pressures (equilibrium oxygen pressures over the metal oxide mixtures) is given in Table 4. Neglecting the disagreement due to different measurement techniques, each separate set of the results obtained within a single research project (e.g., [18, 50, 51]) shows the following trends:

1. Introduction of REE dopant cations into the bismuth oxide lattice results in a definite enlargement of the stability range, with the decomposition limits moving to lower oxygen pressures with increasing dopant content.
2. The most effective additions to enlarge the stability domains are higher-valency metal oxides such as WO_3.
3. No doping leads to a key improvement of the stability of Bi_2O_3-based oxides, as their decomposition still occurs at considerably high oxygen pressures with respect to solid electrolytes based on ZrO_2 [1], HfO_2 and CeO_2 [3].

Table 4 Low-oxygen-pressure stability limits for some Bi_2O_3-based phases

Composition	$-\log p(O_2)$ (atm)		Ref.
	873 K	973 K	
Bi_2O_3	8.25 ± 0.43	5.94 ± 0.40	[18]
	10.96 ± 0.03	8.94 ± 0.03	[50]
	13.01 ± 0.02	10.80 ± 0.04	[51]
$Bi_{0.75}Y_{0.25}O_{1.5}$	13.45 ± 0.10	11.09 ± 0.08	[51]
	9.35 ± 0.43	6.96 ± 0.40	[18]
$Bi_{0.70}Y_{0.30}O_{1.5}$	13.80 ± 0.07	11.43 ± 0.05	[51]
	9.24 ± 0.43	6.78 ± 0.40	[18]
$Bi_{0.63}Y_{0.37}O_{1.5}$	14.23 ± 0.10	11.80 ± 0.08	[51]
$Bi_{0.80}Er_{0.20}O_{1.5}$	11.47 ± 0.03	9.04 ± 0.03	[50]
$Bi_{0.73}Er_{0.27}O_{1.5}$	13.63 ± 0.10	11.30 ± 0.08	[51]
$Bi_{0.68}Er_{0.32}O_{1.5}$	14.01 ± 0.10	11.56 ± 0.08	[51]
$Bi_{0.63}Er_{0.37}O_{1.5}$	14.55 ± 0.10	11.92 ± 0.08	[51]
$Bi_{0.70}Dy_{0.30}O_{1.5}$	13.60 ± 0.07	11.18 ± 0.04	[51]
$Bi_{0.65}Dy_{0.35}O_{1.5}$	13.90 ± 0.10	11.44 ± 0.08	[51]
$Bi_{0.60}Dy_{0.40}O_{1.5}$	14.31 ± 0.10	11.71 ± 0.08	[51]
$Bi_{0.80}Er_{0.10}La_{0.10}O_{1.5}$	9.04 ± 0.43	6.66 ± 0.40	[18]
$3(Bi_2O_3)\cdot(BaO)$	9.22 ± 0.43	6.86 ± 0.40	[18]

Ionic transport

The pioneering work of Neuimin et al. [60] showed for the first time the presence of oxygen ionic conductivity in Bi_2O_3-based ceramics. In general, as found for the δ-phase of Bi_2O_3, the oxides with stabilized fcc structure in the Bi_2O_3-Ln_2O_3 systems (often referred to as δ*-phases) exhibit a very high ionic conductivity (Fig. 2). The oxygen ionic transport in these materials is predominant; as a rule, the electron transference numbers are less than 0.1 [18, 39, 47, 50, 54].

A comment is needed on the δ-phase decomposition processes, caused by the above-mentioned metastability

of the fcc phases. The result of this process is a degradation of the conductivity with time, but at a relatively slow rate [40, 41, 59]. Therefore, the experimentally observed trends of the ionic conductivity correspond very often to the phase thermodynamically stable in the high-temperature range (870–1170 K) but metastable at lower temperatures. The term "stabilized δ-phase" relates to such materials. Also, most of the reported data was not affected by phase decomposition, since the time required for a single experiment is small relative to the period needed to reach significant degradation. For example, the values of the ion transference numbers of $Bi_{0.8}Er_{0.2}O_{1.5}$ at 573–640 K, measured by a relatively time-consuming technique (a modified e.m.f. method, using argon [64]), were found to be still equal to 0.99–1.00 [50], while a drop in the ionic contribution would be expected in the case of phase decomposition. In addition, in many cases the phase composition was checked both before and after the experiments [47].

The ionic conductivity of solid solutions with a stabilized fcc structure was found to decrease with increasing concentration of the stabilizing dopant [18, 47], which is associated with a decreasing unit-cell volume and an increasing average strength of the cation-anion bonds. The highest conductivity is found for materials containing minimum additions necessary to stabilize the δ-phase (the so-called minimum stabilization limit). Such a trend determines the dependence of the oxygen ionic conductivity of δ-Bi_2O_3-based oxides on the radii of dopant cations, discussed in detail in several papers [4, 5, 6, 7, 8, 9]. Namely, the ionic conduction increases with increasing REE dopant radii, but the minimum stabilization limit also increases with the radii; the latter tendency leads to a decrease in ionic transport of the most-conductive materials with increasing radii of the stabilizing cations. As a result, the conductivity dependence on the REE radii exhibits a maximum, corresponding to Er^{3+} and Y^{3+}. The highest ionic conductivity in the binary Bi_2O_3-Ln_2O_3 systems was reported for the $Bi_{1-x}Er_xO_{1.5}$ ($x \approx 0.20$) and $Bi_{1-x}Y_xO_{1.5}$ ($x = 0.23$–0.25) solid solutions [18, 39, 47, 50].

Electronic conductivity

Table 5 lists the values of oxygen ion transference numbers (t_o) for selected Bi_2O_3-based ceramics at oxygen partial pressures close to atmospheric air, determined by the e.m.f. method. Significant polarization resistance of the electrodes [65] and oxygen permeability of the sample under study [39] may influence the transference number determinations by this technique. The effect of polarization resistance leads to measured t_o values lower than the true quantities [65], and typically increases with decreasing temperature. This influence is certainly important for Bi_2O_3-based materials since their reaction with electrodes [18, 59] may increase the polarization resistance to a considerable extent. In addition, interaction between electrolyte and electrode materials leads very often to an increase in electronic transport and to the appearance of a parasitic e.m.f. The influence of oxygen permeability on the e.m.f. results, owing to a local deviation of oxygen chemical potentials from the ideal values, depends on both ionic and electronic conductivities and increases with temperature [39]. An additional source of error is the phase metastability, as previously mentioned. As a result, typical values presented in Table 5 show errors as high as $\pm(0.02$–$0.03)$. Obviously, similar errors are also typical for other measurement techniques. In particular, the easy reducibility of bismuth oxide phases may result in errors in Faradaic efficiency results owing to reduction of the samples by the applied electric field [41, 48], while oxygen permeability data may be affected by interaction of bismuth oxide with other materials from the measuring cells.

Irrespective of the above-mentioned constraints, a few trends in electronic transport in δ-Bi_2O_3-based solid solutions can be determined. Firstly, most Bi_2O_3-based ceramics are characterized by a significant p-type electronic contribution in air. This was confirmed not only by transference number measurements, but also by data on the oxygen partial pressure dependence of the total conductivity (for example, see [39]). Such a feature considerably limits the possible application of Bi_2O_3-based materials in sensors, but leads to large oxygen surface exchange rates with respect to other solid electrolytes, as described below. Secondly, most bismuth-containing ceramics are characterized by a low activation energy for electronic transport (in comparison with that of ionic conduction), which results in decreasing ion transference numbers with decreasing temperature (Table 5). This tendency is noticed mostly in materials where a segregation occurs at the grain boundaries of electronically conducting phases such as $BaBiO_{3-\delta}$, $Bi_2CuO_{4\pm\delta}$ or PrO_x. However, other oxides also exhibit similar trends. Even the segregation of a ZrO_2-based phase, having relatively low ionic and electronic conductivities (in the case of Zr-doped $Bi(Y)O_{1.5}$ [63]), provides no abatement of electronic conduction.

Synthesis and thermal expansion

Data on the kinetics of solid state reactions and polymorph transformations in the systems Bi_2O_3-Ln_2O_3 (Ln = Y, Sm, Ho, Er) may be found in several papers [18, 66, 67, 68] and references therein. Among the most interesting results, one should note an observation [67] reporting that an external electric field increases the rate of solid state interaction between Bi_2O_3 and Y_2O_3 at temperatures below the $\alpha \rightarrow \delta$ transition temperature, while further heating leads to independence of the reaction rate on electrical potential difference. As for other oxide solid electrolytes [1, 2, 3], processing conditions affect transport properties of Bi_2O_3-based ceramics to a

Table 5 Oxygen ion transference numbers for Bi_2O_3-based ceramics measured by the e.m.f. method under an oxygen partial pressure gradient of 1.0/0.21 atm

Composition	Phase composition[a]	T (K)	t_o	Ref.
$Bi_{0.90}Nb_{0.10}O_{1.5}$	δ	950	0.97	[40]
		923	0.98	
		860	0.96	
$Bi_{0.84}Nb_{0.16}O_{1.5}$	δ	950	0.96	[40]
$(Bi_{0.95}Nb_{0.05})_{0.85}Ho_{0.15}O_{1.5}$	δ	973	0.96	[41]
		928	0.96	
		882	0.98	
$Bi_{0.75}Y_{0.25}O_{1.5}$	δ	1050	0.99	[61]
		850	0.98	
		750	0.96	
$Bi_{0.75}Y_{0.25}O_{1.5}$	δ	973	0.91	[39]
		873	0.89	
		773	0.83	
$Bi_{0.80}Er_{0.20}O_{1.5}$	δ	973	0.90	[39]
		873	0.88	
		773	0.85	
$Bi_{0.75}Y_{0.25}O_{1.5}$ + 7.2 mol% CuO	δ + I	1050	0.91	[61]
		950	0.84	
		850	0.57	
$Bi_{0.75}Y_{0.25}O_{1.5}$ + 21.1 mol% CuO	δ + I	1050	0.90	[61]
		950	0.81	
		850	0.43	
$0.9BiYO_3 + 0.1BaO$	δ + I	950	0.76	[62]
		850	0.61	
		750	0.39	
$(Bi_{0.75}Y_{0.25}O_{1.5})_{0.9}(ZrO_2)_{0.1}$	δ + Zr	1053	0.98	[63]
		973	0.93	
		873	0.85	
$(Bi_{0.60}Y_{0.40}O_{1.5})_{0.9}(ZrO_2)_{0.1}$	δ + Zr + I	1053	1.00	[63]
		973	0.96	
		873	0.93	
$(Bi_{0.95}Zr_{0.05}O_{1.525})_{0.85}(YO_{1.5})_{0.15}$	δ	873	0.98	[46]
$(Bi_{0.95}Zr_{0.05}O_{1.525})_{0.80}(YO_{1.5})_{0.20}$	δ	873	1.00	[46]
$(Bi_{0.75}Y_{0.25}O_{1.5})_{0.95}(PrO_{1.83})_{0.05}$	δ	1070	0.92	[44]
		950	0.86	
		793	0.78	
$(Bi_{0.60}Y_{0.40}O_{1.5})_{0.95}(PrO_{1.83})_{0.05}$	δ	1070	0.93	[44]
		950	0.95	
		793	0.90	
$(Bi_{0.70}Co_{0.30})_{0.90}Y_{0.10}O_{1.5}$	δ	1050	0.96	[45]
$(Bi_{0.90}Pb_{0.10})_{0.80}Y_{0.20}O_{1.5}$	δ	950	0.90	[43]
		800	0.89	
$(Bi_{0.90}Pb_{0.10})_{0.75}Y_{0.25}O_{1.5}$	δ	950	0.91	[43]
		800	0.93	
$(Bi_{0.68}Pb_{0.32})_{0.85}Y_{0.15}O_{1.5}$	δ	800	0.94	[43]
		730	0.92	

[a] δ corresponds to the fcc phase of Bi_2O_3; Zr corresponds to the zirconia-based cubic fluorite-type phase; I corresponds to other phase impurities

considerable extent. For example, the conductivity of the $Bi_{0.70}Y_{0.30}O_{1.5}$ electrolyte prepared by microwave fusion in a cold container [69] was similar to that of the most-conducting Bi_2O_3-Y_2O_3 solid solutions [18, 54].

Thermal expansion coefficients of stabilized fcc phases are comparable with those of δ-Bi_2O_3, varying in the range 14×10^{-6} to 24×10^{-6} K^{-1} (Table 3). This considerably limits the number of possible electrode materials compatible with Bi_2O_3-based solid solutions [46]. The only electrode materials having similar TECs are doped perovskite-type cobaltites, $LnCoO_{3-\delta}$ [2, 46]. As for pure bismuth oxide, an obvious correlation between thermal expansion and ionic conductivity of the Bi_2O_3-containing ceramics appears in the experimental data [18, 36, 39, 47].

Ion-conducting phases in the systems Bi-M^{VI}-O (M=W, Mo)

Phase relationships, stability and crystal structure

Phase diagrams, selected phase relationships and crystal structures of the separate oxide compounds have been reported for the binary Bi_2O_3-WO_3 [70, 71, 72, 73, 74, 75, 76, 77, 78, 79, 80] and Bi_2O_3-MoO_3 [73, 74, 79, 80, 81, 82, 83, 84, 85] and ternary Bi_2O_3-WO_3-MoO_3 [74, 79, 80] systems. Thermodynamic and structural data on these oxides can also be found in articles on more complex systems such as Bi_2O_3-TeO_2-WO_3 [86], Bi_2O_3-TiO_2-WO_3 [87], Bi_2WO_6-$Bi_4Ti_3O_{12}$ [88], Bi_2WO_6-Bi_5N-

b_3O_{15} [89], Bi_2WO_6-Bi_2GeO_5 [90], Bi_2MoO_6-$Bi_4Ti_3O_{12}$ [91] and the sillenite-like phases Bi_2O_3-$MoO_3(WO_3)$-$MeO(Me_2O_3)$ where Me corresponds to various di- and trivalent metals [92]. Also, the crystal chemistry and polymorphism of the aurivillius family $(Bi_2O_2)^{2+}(A_{n-1}B_nO_{3n+1})^{2-}$ layered compounds were discussed using examples from the Bi_2O_3-WO_3 and Bi_2O_3-TiO_2-WO_3 systems [93, 94, 95, 96]. Selected data on the kinetics of solid state synthesis and on the properties of melts and thin films are available ([97, 98, 99, 100] and references therein).

In the system Bi_2O_3-WO_3, five compounds ($Bi_{12}WO_{21}$, Bi_6WO_{12}, Bi_4WO_9, Bi_2WO_6 and $Bi_2W_2O_9$) were reported [76]. The solid solubility of tungsten oxide in the monoclinic Bi_2O_3 α-phase as well as the possible formation of metastable tetragonal β*- and fcc δ*-phases are found in the Bi-rich part of the phase diagram [70, 76, 77, 78]. Generally, crystal structures of all Bi_2O_3-WO_3 phases may be considered as fluorite related [78]. The most stable compounds in this system, Bi_6WO_{12} and Bi_2WO_6, which might be of interest as oxygen ionic conductors, possess relatively narrow solid-solution domains ($\sim$8 mol% and 1–1.5 mol%, respectively) [70, 76, 77, 78]. The unit cell of Bi_6WO_{12} at low temperature is fluorite-like face-centered cubic with the lattice parameter $a\approx0.55$ nm [70, 73, 78]; at approximately 1170 K, this solid solution shows a phase transition probably due to disordering [70, 76, 78]. Bi_2WO_6 at room temperature has a rhombically distorted layered polar structure (space group *Aba*2 or *Pba*2), which transforms into a monoclinic fluorite-related lattice (space group *C*2/*m*) at 1233 K [75, 76, 80]. Note that the phase transitions in both Bi_6WO_{12} and Bi_2WO_6 are associated with significant volume changes, leading to sample destruction [75, 76].

In the Bi_2O_3-MoO_3 system there are seven compounds with Bi:Mo ratios equal to 12:1, 6:1, 4:1, 3:1, 2:1, 1:1 and 2:3 [13, 80, 83, 85, 101]. Analogously to the Bi_2O_3-WO_3 oxides, the phases Bi_6MoO_{12} and Bi_2MoO_6 are more stable with respect to other compounds and exhibit reversible phase transitions when heated; the polymorph transformation temperatures in this case are 1138 and 873–883 K, respectively [13, 79, 80, 81]. As for Bi_2WO_6, the crystal structure of the low-temperature modification of Bi_2MoO_6 (the so-called γ-phase) is layered rhombically distorted (space group $P2_1/c$); the high-temperature polymorph (γ'-Bi_2MoO_6) has a monoclinic lattice (space group *C*2/*m*) [80]. Such similarity between Bi_2WO_6 and Bi_2MoO_6 leads to significant mutual solid solubility of these compounds [74, 79, 80]. In particular, the monoclinic γ'-$Bi_2Mo(W)O_6$ solid solutions exist up to $\sim$15% tungsten in the molybdenum sublattice, at 1200 K [80], while in the case of the γ-phase this range is as large as 70% [74]. It should also be noted that both Bi_2WO_6 and Bi_2MoO_6 are characterized by cation nonstoichiometry in the bismuth sublattice [81], which may lead to formation of oxygen vacancies and/or extended defects, thus increasing the oxygen mobility.

If compared to undoped bismuth oxide, materials of the Bi_2O_3-WO_3 system exhibit a better stability with respect to volatilization [102] and reduction at low oxygen pressures (Table 4). However, such improvements are relatively small and do not result in performance comparable to zirconia or ceria. For example, bismuth depletion of the surface layer of $(Bi_2O_3)_{0.78}(WO_3)_{0.22}$ ceramics in the course of annealing started at 920 K [102], whereas significant evaporation of bismuth oxide in the case of undoped Bi_2O_3 starts at approximately 700 K [103, 104]. Consequently, the Bi_2O_3-based materials high-temperature applicability limit in air corresponds to 920–970 K; decreasing oxygen partial pressure down to $\sim$1 Pa lowers this limit to values of about 820 K [102].

Transport properties

In a pioneering article, Yushina and Palguev [105] demonstrated a high oxygen ionic conductivity in Bi_2O_3-MoO_3 ceramics, as well as non-negligible ionic transport in MoO_3 and PbO. Data on electrical properties were published for ceramics and single crystals of Bi-W-O [70, 71, 72, 81, 106, 107], Bi-Mo-O [80, 81, 82, 105, 106] and Bi-W-Mo-O [80] systems, and some complex aurivillius-type compounds containing bismuth and tungsten oxides [88, 89, 93, 94, 96, 108]. The maximum conductivity, which is predominantly ionic and decreases with increasing tungsten concentration, was reported for the fcc solid solutions in the system Bi_2O_3-WO_3 [70]. However, the phase stability of these materials at low temperatures may be questionable. The Bi_2WO_6 phase exhibits a low conductivity with respect to the fluorite-like solid solutions [72, 81, 107], but the oxygen ion transference numbers of Bi_2WO_6 in oxidizing conditions are still close to unity (Fig. 3). Notice that the values of the transference numbers given in Fig. 3 were measured using the e.m.f. method and therefore may be significantly affected by factors mentioned in the previous section. Decreasing the oxygen partial pressure down to 10^{-2}–10^{-3} atm results in a sharp increase in the n-type electronic conductivity of Bi_2WO_6 [81, 107]. Similar dependencies of transport properties on oxygen pressure are observed for other phases in the systems Bi-Mo-O (Fig. 4) and La-W-O [109].

The Bi_2O_3-MoO_3 compounds, including $Bi_2(MoO_4)_3$ (the so-called α-phase), $Bi_2Mo_2O_9$ (β-phase), γ- and γ'-Bi_2MoO_6, possess a mixed ionic-electronic conductivity in oxidizing conditions at 670–900 K [80, 81, 82]. Their total conductivity at oxygen pressures close to atmospheric air increases in the sequence $Bi_2(MoO_4)_3 < Bi_2Mo_2O_9 < \gamma'$-$Bi_2MoO_6 \leq \gamma$-$Bi_2MoO_6 < Bi_2WO_6$ [81]. The β- and γ-phases in these conditions exhibit predominant ionic conduction, while the α-phase is an electronic conductor. Such changes in the ionic transport correlate with the catalytic activity and the coordination number of molybdenum cations in the crystal lattice; a possible explanation for this behavior is the

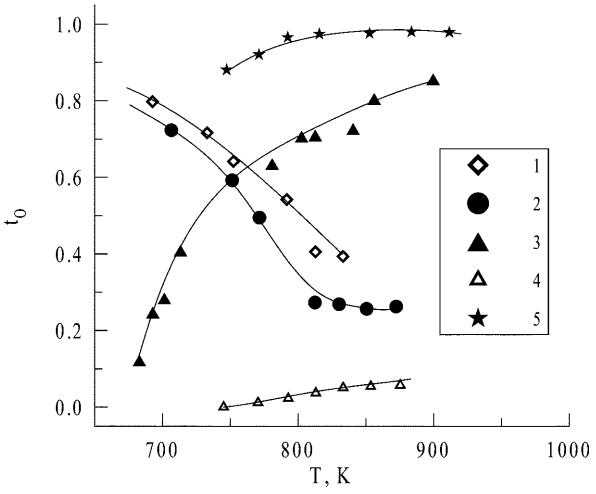

Fig. 3 Temperature dependence of the ion transference numbers measured by the e.m.f. method at an oxygen pressure gradient of 1.0/0.21 atm: *1*, γ-Bi_2MoO_6; *2*, $Bi_2Mo_2O_9$; *3*, γ'-Bi_2MoO_6; *4*, $Bi_2(MoO_4)_3$; *5*, Bi_2WO_6. The data from [81] are used in the figure

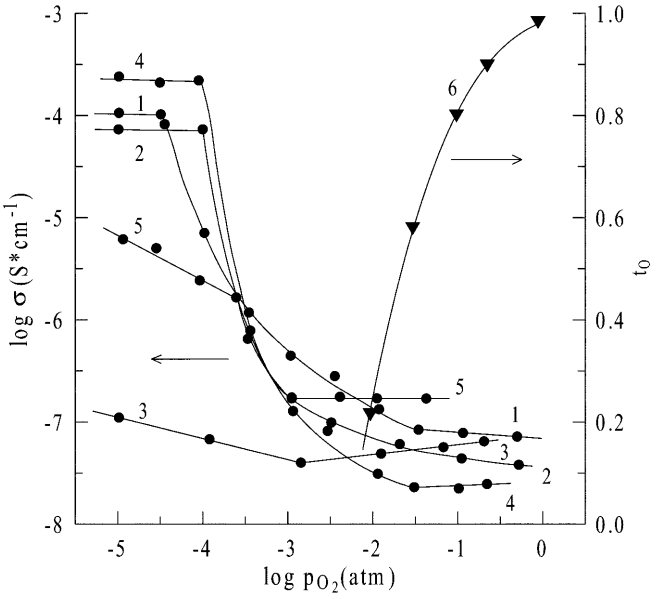

Fig. 4 Oxygen partial pressure dependence of the total conductivity at 673 K (*1–5*) and oxygen ion transference numbers at 1003 K (*6*): *1*, γ-Bi_2MoO_6; *2*, $Bi_2Mo_2O_9$; *3*, γ'-Bi_2MoO_6; *4*, $Bi_2(MoO_4)_3$; *5* and *6*, Bi_2WO_6. The data from [81] and [107] are used. The *solid lines* are for visual guidance only

formation of extended defects from Mo-O octahedra bonded into chains in the structure of the γ-phase [81, 82]. Reducing the oxygen pressure down to 10^{-5} atm leads to a larger n-type electronic conductivity, which increases as $\gamma' < Bi_2WO_6 < \beta \leq \gamma < \alpha$ [81, 82].

Lastly, the results on the electrical properties of some Bi_2O_3-containing solid solutions [89, 93, 96], belonging to the aurivillius series, demonstrate their relatively high conductivity, presumably ionic. The crystal lattice of the oxides of the aurivillius family, $(Bi_2O_2)^{2+}(A_{n-1}B_nO_{3n+1})^{2-}$, consists of alternating bismuth oxide and perovskite-like layers; an example of the end members of this family ($n=1$) may be represented by Bi_2WO_6 [72, 93, 96]. Significant ionic transport in such compounds may occur owing to the presence of oxygen vacancies and extended defects in the perovskite layers. For instance, the total electrical conductivity at 673 K is as high as 3×10^{-4} S cm^{-1} for $Bi_{10}Ti_3W_3O_{30}$ [93] or 1×10^{-4} S cm^{-1} for $0.88Bi_2WO_6$-$0.12Bi_5Nb_3O_{15}$ [89]. However, there is no proof of the fact that this conduction is ionic. In fact, all conclusions are based on the analysis of the crystal structure and data on total conductivity.

Bi_2O_3-M_2O_5 systems (M=P, V, Nb, Ta)

Phase diagrams, separate phase relationships as well as structural, thermodynamic and optical properties of some oxide phases have been published for the binary systems Bi_2O_3-M_2O_5, where M = P [13, 110, 111, 112, 113], V [13, 90, 110, 114, 115, 116, 117, 118, 119, 120, 121, 122], Nb or Ta [40, 73, 123, 124], and for several more complex systems such as $Bi_4GeVO_{10.5}$ and $Bi_8P_{4-x}Ge_{1+x}O_{24-x/2}$ [125], $Bi_4V_2O_{11}$-Bi_2GeO_5 and $Bi_4V_2O_{11}$-Bi_2WO_6 [90], Bi_2O_3-V_2O_5-PbO [114], Nb-containing aurivillius phases [89, 96] and sillenite- and pyrochlore-type compounds [118, 126, 127]. Data on Bi_2O_3-M_2O_5 phases are characterized by significant disagreement, which is associated, in particular, with a variety of metastable states and possible volatilization of components such as bismuth, vanadium and phosphorus oxides in the course of sample preparation. In addition, the oxidation-reduction processes, which occur easily in the system Bi-V-O, prevent the treatment of this system as simple pseudobinary (Bi_2O_3-V_2O_5), even under oxidizing conditions [117].

For the bismuth-rich part of the Bi_2O_3-P_2O_5 system, six compounds with Bi:P ratios of 25:1, 12:1, 5:1, 3:1, 2:1 and 1:1 have been reported [13, 113]. In addition, the compounds 1:2, 1:3, 1:4 and 1:5 (Bi:P) were prepared from phosphorous acid melts [111]. The sillenite-type phases $Bi_{24}[Bi^{3+}P]O_{40}$ and $Bi_{24}P_2O_{41}$ exhibit negligible mutual solid solubility, caused by a high enthalpy of solid-solution formation when bismuth is substituted by pentavalent phosphorus [112]. Katkov et al. [110] reported the existence of $Bi_{12}P_2O_{23}$; single crystals of $Bi_4P_2O_{11}$ and $Bi_{12}P_2O_{23}$ have a monoclinic structure with space group $C2/c$ or Cc for $Bi_4P_2O_{11}$ and $P2_1$ or $P2_1/m$ for $Bi_{12}P_2O_{23}$ [110].

In the Bi-rich part of the Bi_2O_3-V_2O_5 phase diagram, five compounds were found, with the Bi:V ratios equal to 12:1, 6:1, 3:1, 2:1 and 1:1 [13, 120]. There is also data on a 4:1 compound, with hexagonal structure [117, 119]. Most of these phases represent solid solutions; their homogeneity domains vary from 0.5 to 4–5 mol% even at low temperatures [13, 119, 120]. The $Bi_{24}V_2O_{41}$ sillenite-type phase decomposes at 1033–1038 K, forming monoclinic $Bi_{12}V_2O_{23}$ and a fluorite-type δ-Bi_2O_3-based solid solution [13, 119, 120]. The $Bi_4V_2O_{11}$ compound belongs to the aurivillius family ($n=1$) and has an

orthorhombic lattice (α-phase) at room temperature, which can be considered as an ordered modification of the high-temperature tetragonal γ-polymorph [117, 122]. On heating $Bi_4V_2O_{11}$, the $\alpha \rightarrow \beta$ and $\beta \rightarrow \gamma$ phase transitions take place at 713 and 823 K, respectively, while the large thermal hysteresis on cooling may decrease the polymorph-transformation temperatures down to 638 and 663 K, correspondingly [117]. Incongruent melting of this bismuth vanadate occurs at 1153 K [13, 117]. A brief summary of the Bi_2O_3-V_2O_5 phases is given in Table 6.

Metastable solid solutions based on the bismuth oxide fluorite-like δ- and sillenite-type γ-phases can be easily obtained in the Bi_2O_3-V_2O_5 system [120]. For example, quenching of solid phases and melts leads to formation of the fluorite phase in the range 8.8–11.5 and 7.2–12.1 mol% V_2O_5, respectively [120]. This suggests that some results on single crystals, obtained from melts (for example [119]), correspond probably to a metastable phase composition.

As for the Bi_2O_3-P_2O_5 and Bi_2O_3-V_2O_5 systems, the fluorite-type δ-Bi_2O_3-based solid solutions exist also in the Bi_2O_3-Nb_2O_5 system [40, 123]; this phase is, however, metastable at temperatures below 900 K [40]. After preparation by the standard ceramic synthesis route, the minimum addition of niobia necessary to stabilize the fluorite phase was found to be approximately 10 mol% [40]. The maximum niobia content in the fcc phase is 23.5 mol% [123, 128]. When annealed at $T < 900$ K for a sufficiently long time, all the Bi_2O_3-Nb_2O_5 solid solutions exhibit phase decomposition, resulting in a conductivity drop [40]. Additions of Nb were shown to increase the stability of bismuth oxide-based materials with respect to reduction at low oxygen partial pressures, as illustrated by Fig. 5. Figure 5 presents also the values of the redundant chemical potential of bismuth oxide $\Delta\mu^{add}(Bi_2O_3)$ in the $(Bi_2O_3)_{1-x}(Nb_2O_5)_x$ solid solutions, calculated as [123]:

$$\Delta\mu^{add}(Bi_2O_3) = \Delta\mu(Bi_2O_3) - RT\ln(1-x) \quad (5)$$

where $\Delta\mu(Bi_2O_3)$ is the chemical potential of bismuth oxide in the reaction of its dissolution in the fluorite lattice:

$$\frac{1}{\alpha}(Bi_2O_3)_{1-x-\alpha}(Nb_2O_5)_x + Bi_2O_3 \underset{\alpha \rightarrow 0}{\longleftrightarrow} \frac{1}{\alpha}(Bi_2O_3)_{1-x}(Nb_2O_5)_x \quad (6)$$

The redundant chemical potential characterizes a deviation from the ideal solution, where $\Delta\mu^{add}(Bi_2O_3) = 0$. In contrast to bismuth oxide stabilized with REE additions [129], the $Bi(Nb)O_{1.5+\delta}$ solid solutions are non-ideal, and the deviation from ideality increases with increasing niobia concentration in the $Bi(Nb)O_{1.5+\delta}$ phase [123]. Thermal expansion coeffi-

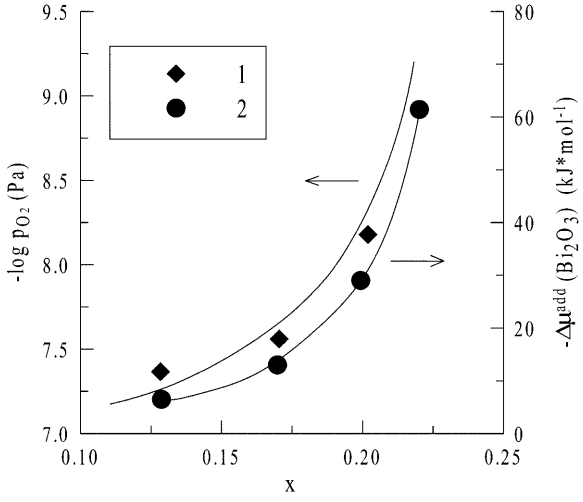

Fig. 5 Concentration dependencies of the stability limit at low oxygen partial pressure (*1*) and the redundant chemical potential of bismuth oxide (*2*) in the $(Bi_2O_3)_{1-x}(Nb_2O_5)_x$ solid solutions at 923 K [123]

Table 6 Properties of oxide phases in the system Bi_2O_3-V_2O_5

Bi:V ratio	Structure	Lattice parameters	Ref.	Phase changes		Ref.
				Process	T(K)	
12:1	bcc cubic	–	[120]	Decomposition	1038	[120]
6:1	Monoclinic	$a = 2.0007$ nm, $b = 1.1549$ nm, $c = 1.9836$ nm, $\beta = 96.63°$	[110]	Congruent melting	1213	[117]
4:1	Hexagonal	$a = 0.381$ nm, $b = 0.998$ nm	[119]	Incongruent melting	1193	[117]
3:1				Incongruent melting	1164	[13]
2:1	Orthorhombic	$a = 1.684$ nm, $b = 1.662$ nm, $c = 1.530$ nm	[122]	Incongruent melting	1153	[13]
				$\alpha \rightarrow \beta$	713	[117]
				$\beta \rightarrow \gamma$	828	[117]
1:1	Orthorhombic	–	[114]	Congruent melting	1213	[13]
				$\alpha \rightarrow \beta$	528	[117]

cients of some $(Bi_2O_3)_{1-x}(Nb_2O_5)_x$ ceramics are given in Table 3.

Selected results on the transport properties of V-, Nb- and Ta-containing phases have been published [40, 89, 93, 96, 115, 125, 127, 130, 131, 132, 133]. These oxides were mainly considered as materials for technical applications such as electronics, and no detailed electrochemical characterization was carried out. For the fluorite-like solid solutions $(Bi_2O_3)_{1-x}(Nb_2O_5)_x$, the conductivity in oxidizing conditions is predominantly ionic; the oxygen ionic conduction decreases with increasing niobia content (Table 7). As for δ-Bi_2O_3 stabilized with REEs [39], p-type electronic conduction is also typical for $Bi(Nb)O_{1.5+\delta}$ in air [40]. However, the electron transference numbers of the niobia-stabilized phases are less than 0.05 (Table 5).

After the pioneering work of Mairesse et al. [134, 135], a number of articles [48, 136, 137] were focused on the properties of γ-$Bi_4V_2O_{11}$, which may be stabilized down to room temperature by partial substitution of vanadium with other metals such as copper or nickel, resulting in unusually high ionic conductivity at 500–800 K. Data on such materials are considered in the section devoted to ternary solid electrolyte oxide systems.

Bi_2O_3-MO_2 oxide systems (M=Si, Ti, Ge, Se, Zr, Ru, Sn, Te, Ir, Pt)

Thermodynamic and structural data, including phase diagrams and selected phase relationships, have been published for the systems Bi_2O_3-SiO_2 [13, 138, 139, 140, 141], Bi_2O_3-TiO_2 [13, 140, 142, 143], Bi_2O_3-GeO_2 [13, 141, 144, 145, 146, 147, 148, 149], Bi_2O_3-SeO_2 [150], Bi_2O_3-RuO_2 [151, 152, 153], Bi_2O_3-SnO_2 [13, 146, 154], Bi_2O_3-TeO_2 [86, 155, 156], Bi_2O_3-IrO_2 [157] and Bi_2O_3-PtO_2 [13]. In addition, some results can be found in articles devoted to ternary systems such as $Bi_{12}SiO_{20}$-$Bi_{12}TiO_{20}$ and $Bi_{12}GeO_{20}$-$Bi_{12}TiO_{12}$ [158], $Bi_{12}SiO_{20}$-$Bi_{12}GeO_{20}$ [159], Bi_2O_3-TiO_2-PbO [143], Bi_2O_3-GeO_2-Me_2O_5 (Me = Nb, Ta) [160], Bi_2O_3-Ga_2O_3-MO_2 (M = Si, Ge) [161], Bi_2O_3-CdO-GeO_2 [148], Bi_2O_3-

Table 7 The total electrical conductivity of Bi_2O_3-based ceramics

Composition	Conductivity (S cm^{-1})		Activation energy		Ref.
	700 K	1000 K	T (K)	E_a (kJ mol^{-1})	
$(Bi_2O_3)_{0.8}(Er_2O_3)_{0.2}$	–	0.54	400–550	151	[39]
			550–800	58	
$(Bi_2O_3)_{0.75}(Y_2O_3)_{0.25}$	1.9×10^{-3}	0.27	600–900	93	[18]
			910–1010	72	
$(Bi_2O_3)_{0.70}(Y_2O_3)_{0.30}$	5.6×10^{-4}	0.16	650–950	97	[18]
			970–1080	77	
$(Bi_2O_3)_{0.60}(Y_2O_3)_{0.40}$	2.3×10^{-4}	9.3×10^{-2}	660–980	113	[18]
			1020–1100	–	
$(Bi_{0.75}Y_{0.25}O_{1.5})_{0.95}(PrO_{1.833})_{0.05}$	1.9×10^{-3}	0.19	630–1050	101	[47]
$(Bi_{0.75}Y_{0.25}O_{1.5})_{0.85}(PrO_{1.833})_{0.15}$	1.9×10^{-4}	2.7×10^{-2}	630–1050	99	[47]
$(Bi_{0.70}Y_{0.30}O_{1.5})_{0.90}(PrO_{1.833})_{0.10}$	1.6×10^{-4}	2.5×10^{-2}	600–1050	97	[47]
$(Bi_{0.60}Y_{0.40}O_{1.5})_{0.90}(PrO_{1.833})_{0.10}$	7.2×10^{-4}	0.12	560–1100	99	[47]
$(Bi_{0.5}Y_{0.5}O_{1.5})_{0.70}(ZrO_2)_{0.30}$	3.3×10^{-5}	6.8×10^{-3}	610–1050	107	[47]
$(Bi_{0.95}Zr_{0.05}O_{1.525})_{0.85}(YO_{1.5})_{0.15}$	1.7×10^{-2}	0.64	520–1070	89	[46]
$(Bi_{0.95}Zr_{0.05}O_{1.525})_{0.80}(YO_{1.5})_{0.20}$	4.8×10^{-3}	0.42	520–1070	91	[46]
$(Bi_{0.90}Zr_{0.10}O_{1.55})_{0.85}(YO_{1.5})_{0.15}$	1.0×10^{-2}	0.55	520–1070	87	[46]
$(Bi_{0.70}Co_{0.30})_{0.90}Y_{0.10}O_{1.5}$	3.1×10^{-3}	0.32	–	–	[38]
$(Bi_{0.90}Pb_{0.10})_{0.80}Y_{0.20}O_{1.5}$	1.4×10^{-3}	0.26	–	–	[43]
$(Bi_{0.90}Pb_{0.10})_{0.75}Y_{0.25}O_{1.5}$	3.9×10^{-4}	0.14	–	–	[43]
$(Bi_{0.68}Pb_{0.32})_{0.80}Y_{0.20}O_{1.5}$	4.4×10^{-4}	–	–	–	[43]
$Bi_{0.92}Nb_{0.08}O_{1.5+\delta}$	–	0.64	760–840	90	[40]
			840–1100	62	
$Bi_{0.90}Nb_{0.10}O_{1.5+\delta}$	–	0.27	760–1100	93	[40]
$Bi_{0.84}Nb_{0.16}O_{1.5+\delta}$	–	0.15	760–1100	101	[40]
$(Bi_{0.95}Nb_{0.05})_{0.90}Ho_{0.10}O_{1.5+\delta}$	7.4×10^{-3}	0.62	530–800	118	[41]
			800–1070	70	
$(Bi_{0.95}Nb_{0.05})_{0.85}Ho_{0.15}O_{1.5+\delta}$	4.5×10^{-3}	0.46	580–810	119	[41]
			810–1100	73	
$(Bi_{0.92}Nb_{0.08})_{0.90}Ho_{0.10}O_{1.5+\delta}$	2.8×10^{-3}	0.32	560–830	108	[41]
			830–1080	81	
$(Bi_2O_3)_{0.80}(WO_3)_{0.20}$	–	5.1×10^{-2}	–	–	[70]
$(Bi_2O_3)_{0.75}(WO_3)_{0.25}$	–	6.0×10^{-2}	–	–	[70]
$(Bi_2O_3)_{0.80}(SrO)_{0.20}$	5.1×10^{-4}	–	–	–	[60]
$Bi_2V_{0.9}Cu_{0.1}O_{5.5-\delta}$	2.0×10^{-2}	0.17	370–730	66	[48]
			730–1020	45	
$Bi_{1.9}La_{0.1}V_{0.9}Cu_{0.1}O_{5.5-\delta}$	1.5×10^{-2}	0.12	370–700	62	[48]
			700–1010	48	
$Bi_{1.9}Pr_{0.1}V_{0.9}Cu_{0.1}O_{5.5-\delta}$	9.2×10^{-3}	8.7×10^{-2}	390–690	69	[48]
			690–1010	50	

SnO_2-MO_2 (M = Si, Ge) [146, 154], Bi_2O_3-Nb_2O_5-TeO_2 [156], Bi_2O_3-TeO_2-WO_3 [86], $Bi_{12-x}Me_xIrO_{20}$ and $Bi_{2-x}Me_xIr_2O_{7-y}$ (Me = Sr, Ca) [162], Bi_2WO_6-$Bi_4Ti_3O_{12}$ [88, 95], $Bi_4Ti_3O_{12}$-Bi_2MoO_6 [91], Bi_2GeO_5-$Bi_4V_2O_{11}$ [90, 125] and Bi_2GeO_5- Bi_2WO_6 [90]. Work on various aspects of single-crystal preparation, including investigations on melts and single-crystal properties, can be found in various papers [159, 160, 163, 164, 165, 166, 167, 168, 169, 170, 171]. Among other results, one should mention data on the interaction of platinum with Bi_2O_3-MO_2 melts [170], showing that the rate of reaction is determined by the dissolution of PtO_2 and the thermal stability of the compounds forming in the liquid phase. The unique optical, electrical and acoustic properties of some Bi_2O_3-MO_2 (M = Si, Ti, Ge) compounds caused significant attention with respect to their electronic and defect structures [149, 158, 172, 173], their various spectra including IR and NMR [159, 164, 165, 166, 174, 175] and their solid state synthesis kinetics [176, 177].

As for many other oxide systems with bismuth oxide, the Bi_2O_3-MO_2 systems are characterized by the formation of a sillenite phase, $Bi_{12}MO_{20}$, whose stability decreases with the increasing radii of the doping cations [21]. For instance, the $Bi_{12}RuO_{20}$ phase is thermodynamically metastable [153], in contrast to the stable $Bi_{12}SiO_{20}$, $Bi_{12}TiO_{20}$ and $Bi_{12}GeO_{20}$ compounds [139, 143, 147, 159, 178]. The crystal lattice of sillenite consists of tetrahedra, formed by dopant cations and oxygen, placed at the center and corners of the bcc unit cell; the BiO_7 polyhedra are placed between them [118]. Since the tetrahedral cationic positions can be occupied not only by dopant ions but also by Bi^{5+} and Bi^{3+}, formation of the sillenite phases depends on the oxygen partial pressure and thermal pre-history, which determine the oxidation state of bismuth. This feature, and possible stabilization of metastable states in the course of synthesis from melts [179], is the source of some disagreement in the literature on sillenites (e.g., see [138, 144]).

Among other oxides of potential interest as ionic conductors, one can mention phases with the Bi:M ratio equal to 2:1 and 4:3. Their formation is common for M^{4+} cations with moderate radii such as Si, Ge, Ti or Se [138, 139, 142, 143, 144, 147, 150, 178]. Note, however, that Bi_2SiO_5 and Bi_2GeO_5 are metastable, while the 4:3 phase in the Bi_2O_3-SeO_2 system does not exist. The crystal lattice of Bi_2GeO_5 is close to that of aurivillius-type compounds [145]; this phase forms solid solutions with members of the aurivillius family such as $Bi_4V_2O_{11}$ and Bi_2WO_6 [90, 125]. No binary compound forms in the Bi_2O_3-ZrO_2 system, and the mutual solid solubility of monoclinic zirconia and bismuth oxide phases is negligible [47]. Pyrochlore phases $Bi_2M_2O_7$ are formed for M = Sn, Ru, Ir or Pt [13, 146, 150, 151, 152, 153, 157, 162].

The Bi_2O_3-MO_2 phases were mainly studied not from a viewpoint of high-temperature electrochemistry, but for applications in other fields such as electronics and optics. Owing to this, no data can be found on transport properties at elevated temperatures, except for the total conductivity. Results on electrical properties of Bi_2O_3-MO_2 oxides and related materials have been published [125, 131, 149, 158, 159, 162, 173].

The Bi_2O_3-M_2O_3 (M=B, Al, Sc, Ga, In) and Bi_2O_3-MeO_x (Me=Cr, Mn, Fe, Co, Pr, Tb) systems

Formation and properties of the Bi_2O_3-M_2O_3 phases

Selected phase relationships and phase diagrams in the Bi_2O_3-M_2O_3 systems, with M = B [180, 181], Al [182, 183], Ga [183, 184, 185] or In [183, 186, 187] can be found in the literature. Sillenite phases, where the Bi:M ratio is 12:1 (B, Al) or approximately 24:1 (Ga, In), form in all these systems. The latter compounds may be represented as $Bi^{III}{}_{24}[Bi^{V}M^{III}]O_{40}$ [118, 186]; the variable valence of bismuth in such oxides determines the relevance of oxygen pressure and thermal pre-history on their formation. Owing to this reason as well as to non-negligible solid-solution domains [13], published data on sillenite composition are characterized by some disagreement [13, 106, 143]. As for other systems with bismuth oxide, the stability of the sillenites decreases with the increasing ionic radii of M^{3+}. The sillenite phase in the Bi_2O_3-In_2O_3 system is, hence, metastable at room temperature [186], but may be stabilized by additions such as P_2O_5 [118]. For M = Al or Ga, formation of the $BiAlO_3$, $Bi_2Al_4O_9$ and $Bi_2Ga_4O_9$ phases was reported in addition to the sillenite solid solutions [1, 182, 184]. However, formation of the 1:1 phase in the Bi_2O_3-Al_2O_3 system is questionable [188]. Some data on Al- and Sc-containing ternary compounds with the pyrochlore structure have been published [127].

Information available on the transport properties of the title materials is limited. Oxygen ionic conduction was studied only for some Bi_2O_3-In_2O_3 compositions [187]. The ceramics $Bi_{1-x}In_xO_{1.5}$, containing sillenite (γ*-Bi_2O_3) and In_2O_3-based solid solutions, exhibit a mixed ionic-electronic conductivity; the oxygen ion transference numbers of $In_{0.67}Bi_{0.34}O_{1.5}$ are in the range 0.5–0.6 at 850–970 K [187]. Since the conductivity of indium oxide is predominantly electronic (for instance, see [189, 190]), this behavior suggests a significant ionic conductivity of the sillenite phase, which is in agreement with the data on other sillenites considered below.

Oxides in the systems Bi_2O_3-MeO_x (Me = Cr, Mn, Fe, Co) and transport properties

For these systems, phase diagrams and data on separate phase relationships have been published for Me = Cr [191, 192, 193], Mn [193, 194], Fe [192, 195, 196, 197, 198] and Co [37, 38, 45, 193, 199, 200]. In addition, some data on Bi-Me-O compounds are also available in work dealing with the pseudobinary systems $BiFeO_3$-$LnFeO_3$ (Ln = La, Pr) [201, 202], $BiFeO_3$-$LaAlO_3$ [203], Bi_2O_3-

$LiFe_5O_8$ [204], and with sillenite [21, 118, 141] and pyrochlore [127] phases. As a general feature, formation of the sillenite phases is typical for all Bi_2O_3-MeO_x systems, but depends, as could be reasonably expected, on the oxidation state of bismuth and the transition metal cations. For example, the composition of the sillenite phase in the Bi-Mn-O system was reported as $Bi^{III}{}_{24}[Bi^{V}Mn^{III}]O_{40}$ [118] and $Bi^{III}{}_{12}[Mn^{IV}]O_{20}$ [193], whereas no sillenite phase was mentioned for the Bi_2O_3-Mn_2O_3 system [13, 188]. As for other Bi_2O_3-based systems, the sillenite phases are characterized by non-negligible homogeneous solid solution formation domains. In particular, the bcc solid solution $BiO_{1.5}$-$CoO_{1.33}$ was found in the approximate range $(4–7)\pm1$ mol% of cobalt oxide [38, 200], which covers the Bi:Co ratios in the Co-containing sillenite phase of 12:1 [193, 199] and 24:1 [205]. When the transition metal concentration is insufficient to form the γ*-phase, the tetragonal β* and monoclinic α polymorphs exist in the binary systems. Formation of the perovkite-related phases $BiMeO_3$ was reported for Me = Cr [192], Mn [194] and Fe [192, 195, 197, 201, 202]; however, the thermodynamic stability of these compounds is very problematic (for instance, see [188, 191, 193]). Among other oxides which might be of potential interest as mixed conductors, one can list $Bi_2Fe_4O_9$ [192, 195] and the solid solutions Bi_{1-x} $Cr_xO_{1.5+\delta}$ ($x = 0.13–0.25$) with an orthorhombic structure [191].

Electrical properties of the Bi_2O_3-MeO_x phases, including the total conductivity and oxygen ion transference numbers, have been studied [37, 38, 45, 131, 193, 200, 203, 206, 207, 208, 209]. The sillenite phases as well as tetragonal $Bi_{38}CrO_{60}$ were established to exhibit a mixed oxygen ionic and p-type electronic conduction in air [37, 38, 45, 193, 200]; the ionic contribution to the total conductivity increases drastically with temperature, especially at $T > 900$ K (Fig. 6). This behavior is similar to that of pure bismuth oxide when the polymorph transformations take place (Fig. 1). However, with increasing temperature, no phase changes were found by high-temperature XRD for at least Co-containing sillenite [38, 200], suggesting that the increase in ionic conductivity is caused by the oxygen sublattice disordering. The p-type electronic conductivity of the γ*-phase-containing ceramics increases with increasing transition metal dopant content and oxygen partial pressure [37, 45, 200]. The conductivity of bismuth ferrite, $BiFeO_3$, and $BiFeO_3$-based solid solutions [131, 203, 209] is, most probably, predominantly electronic; there are no data available on ionic transport in this phase.

Mixed conductors of bismuth oxide doped with praseodymia and terbia

Data on Bi_2O_3-PrO_x and Bi_2O_3-TbO_x ceramics, including crystal structure, electrical conductivity and transference numbers, as well as estimates on catalytic and electrochemical activity, have been reported [210, 211, 212, 213, 214, 215]. No stabilization of the δ-phase was observed for the system with praseodymia, whilst adding more than 15% of terbium oxide stabilizes the fluorite phase [210, 211]. The metastability of the δ-phase in other Bi_2O_3-Ln_2O_3 systems at low temperatures, considered above, suggests that the fcc $Bi(Tb)O_{1.5+\delta}$ solid solutions are also metastable. As for zirconia-based ceramics doped with variable-valence cations [1], the ability to vary the electronic conductivity of bismuth oxide using praseodymia and terbia additions is limited: the maximum electron transference numbers do not exceed 0.2 for Bi_2O_3-PrO_x and 0.5 for Bi_2O_3-TbO_x [210, 211]. The ionic conduction in the Pr- and Tb-doped ceramics decreases with dopant concentration. When analyzing data [210, 211] on transference numbers, one should note the obvious correlation between ionic and electronic conductivity, which may be caused by experimental errors in transport number determinations, as previously discussed. In particular, a significant polarization resistance of electrodes in the case of e.m.f. measurements [211] might lead to underestimated ion transference numbers [11, 65]; in this case the electronic conductivity values calculated from the measured t_o values is overestimated and correlates to the total conductivity, predominantly ionic.

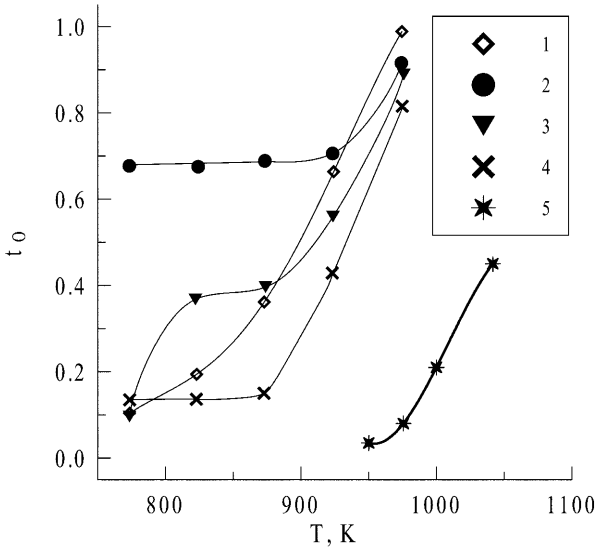

Fig. 6 Temperature dependence of the oxygen ion transference numbers of ceramic samples: *1*, Bi_2O_3; *2*, $Bi_{16}CrO_{27}$; *3*, $Bi_{38}CrO_{60}$; *4*, $Bi_{24}Co_2O_{39}$; *5* $Bi_{0.9}Co_{0.1}O_{1.5}$. The data from [193] and [200] are used

Ion- and electron-conducting phases in the Bi_2O_3-$M^{II}O$ systems

Phase relationships and electrical conduction in Bi_2O_3-MO (M = Ca, Sr, Ba, Pb) ceramics

As for most Bi_2O_3-based systems, the solid state interaction of bismuth oxide with bivalent metal oxides are redox reactions involving oxygen from the gas phase.

Hence, consideration of the title phases in the framework of pseudobinary Bi_2O_3-MO systems is an oversimplified approach, and a correct phase analysis should refer to the ternary Bi-M-O systems. However, experimental results available on the oxygen content in these oxides are limited, owing to the above-mentioned experimental difficulties. As a consequence, most data correspond only to phase compositions equilibrated with oxygen at a given oxygen partial pressure, such as in air. The oxidation state of the bismuth cations is, most often, assumed to be 3+, except in recent data on Ba-Bi-O phases. This assumption will be adopted in this review, following previous work.

The literature contains phase diagrams and data on selected phase relationships, mainly equilibrated with atmospheric air, for the systems Bi_2O_3-CaO [216], Bi_2O_3-CaO-SrO [217, 218, 219], Bi_2O_3-SrO [13, 220, 221, 222], Bi_2O_3-BaO [18, 223, 224, 225, 226, 227] and Bi_2O_3-PbO [77, 83, 181, 228]. Some data on $BaBiO_{3-\delta}$ can also be found [229, 230, 231, 232]. Note that recent work [220, 223, 225, 226, 232] considers the phase composition and structure of some complex oxides of these systems in conjunction with oxygen content and/or oxidation state of bismuth; in particular, Klinkova et al. [225] reported a cross section of the BaO-$BiO_{1.5}$-$BiO_{2.5}$ phase diagram. It should be also mentioned that, as for some other phase diagrams, the results [77, 83, 181, 228] on phase relationships in the Bi_2O_3-PbO system are quite old and much less precise than recent data [233, 234]. For this system, the phase $Bi_8Pb_5O_{17}$ ($Bi_{0.62}Pb_{0.38}O_{1.5\pm\delta}$) may be considered as a promising basis for further modifications in order to develop novel ionic conductors with improved properties [43].

While only magnesia and bismuth oxide phases coexist in the Bi_2O_3-MgO system [13], the phase diagrams Bi_2O_3-MO (M = Ca, Sr, Ba) are much more complex and include, in particular, solid solution domains with rhombohedral structure (so-called β_1 and β_2 phases), a series of layered perovskite-related phases, as well as solid solutions based on the α- and δ-polymorphs of bismuth oxide [18, 215, 216, 217, 218, 219, 220, 221, 222, 223, 224, 225, 226, 227]. The concentration fields for formation of rhombohedral phases, with relatively high and predominant ionic conductivity, lie in the approximate range from 20 to 25–35 mol% MO; the upper limit depends on the temperature and on the oxidation state of the bismuth cations. A typical feature of the rhombohedral $Bi(M)O_{1.5-\delta}$ solid solutions refers to the $\beta_2 \rightarrow \beta_1$ phase transition at 800–1000 K, which is accompanied by a sharp increase in ionic conductivity (Fig. 7) and significant volume changes [18]. The temperature of this phase transformation decreases with increasing radii of the alkaline-earth dopant cations [13]. In the bismuth-rich part of the Bi_2O_3-BaO system, further increase in barium concentration results in the formation of the homologous perovskite-related series $Ba_mBi_{m+n}O_y$; these compounds are unstable at low temperatures and decompose, forming the rhombohedral phase and perovskite-like barium bismuthate, $BaBiO_{3-\delta}$ [223]. Increasing barium content in the Bi_2O_3-BaO ceramics is associated with a permanent increase in p-type electronic conductivity (Fig. 7), which becomes predominant for $BaBiO_{3-\delta}$ [18, 229, 230]. Notice that ionic transport in barium bismuthate is still considerable, providing a significant oxygen permeability of $BaBiO_{3-\delta}$ membranes [229]. As found for Ba-doped bismuth oxide phases, the Bi_2O_3-SrO and Bi_2O_3-PbO oxides also exhibit mixed ionic and p-type electronic conduction in oxidizing conditions [60, 105, 221]; the oxygen ionic contribution to the total conductivity increases, as a rule, with increasing temperature (for example, Table 8). Comparative data on the properties of some Bi_2O_3-MO compositions are given in Tables 3, 4 and 7.

Compounds of bismuth and divalent transition metal oxides (M = Ni, Cu, Zn, Pd, Cd)

Phase diagrams in the systems based on Bi_2O_3 and divalent transition metal oxides are essentially simpler than those with alkaline-earth metals. For the Bi_2O_3-NiO system, there is no evidence for the formation of binary compounds [235]. In the case of M = Cu or Pd,

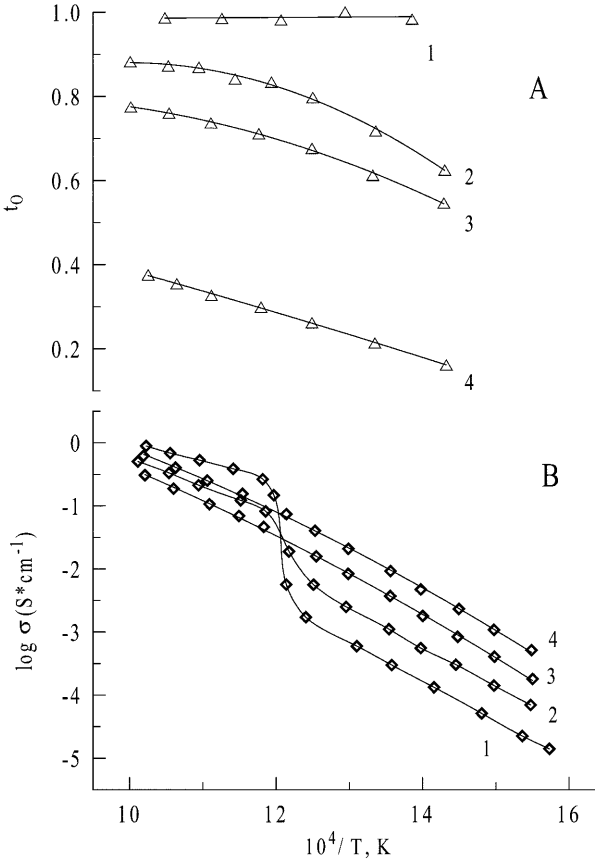

Fig. 7 Temperature dependence of the oxygen transference numbers (**A**) and the total electrical conductivity (**B**) of $(Bi_2O_3)_{1-x}(BaO)_x$ ceramics [18]: *1*, $x = 0.25$; *2*, $x = 0.35$; *3*, $x = 0.40$; *4*, $x = 0.50$

the phase diagrams show the existence of only one phase, Bi_2MO_4 [235, 236, 237, 238, 239, 240], thermodynamically stable at oxygen pressures close to air. The compounds Bi_2CuO_4 and Bi_2PdO_4 are isostructural and form a continuous series of solid solutions [235, 238]. The tetragonal crystal lattice of these oxides was ascribed to the space groups $P4/ncc$ [235, 237, 239] or $P4/mmm$ [18, 241]. Bismuth cuprate possess oxygen hypostoichiometry even at low temperatures in air [242]; heating $Bi_2CuO_{4-\delta}$ leads to increasing δ, which reaches about 3–4% of stoichiometric oxygen content on approaching the melting point (~1123 K) in air [235, 239, 243]. The maximum oxygen hypostoichiometry representing the stability limit of the bismuth cuprate phase was as high as $\delta = 0.5$, corresponding to monovalent copper [243]. Contrary to bismuth cuprate, Bi_2PdO_4 is less stable with respect to oxygen losses and decomposes into metallic Pd and Bi_2O_3 when heated even up to 1078 K in air [235]. Notice that some data on $Bi_2CuO_{4-\delta}$ and derived solid solutions can be found in work on the pseudobinary and ternary systems Bi_2CuO_4-Ln_2CuO_4 [49, 244], Bi_2O_3-SrO-CuO [245] and $Bi_{1.5}Y_{0.5}O_3$-Bi_2CuO_4 [18, 246].

For the Bi_2O_3-ZnO and Bi_2O_3-CdO systems, phase diagrams and the structures of separate phases have been published [148, 247, 248, 249, 250, 251, 252, 253, 254]. In addition, the crystal structure of several sillenite- and pyrochlore-type compounds containing Cd and Zn was studied [21, 118, 127]. One should also mention work [255, 256] devoted to the properties of melts and single crystals of these systems. While formation of Bi_2CdO_4 is observed in the Bi_2O_3-CdO system, zinc oxide does not form the 2:1 compound (Bi:M) with bismuth oxide. However, in contrast to the systems with Ni, Cu and Pd, sillenite phases form when M = Zn or Cd, with filled d-shells [247, 248, 250, 251]. As for other γ^*-Bi_2O_3-based solid solutions, formation of the sillenite phases depends strongly on the bismuth oxidation state and, therefore, on the preparation method and thermal pre-history of the samples; this causes contradictions in the literature on the exact cation composition of the bcc solid solutions [21, 118, 247, 248, 250, 251]. The cadmium-containing sillenite phases forming in atmospheric air have a Bi:Cd ratio equal to 12:1 and 10:3 [148, 248, 249, 250]; the thermodynamic stability of these compounds at temperatures below 900 K may be, however, questionable [13]. An interesting feature of the sillenite-type $5Bi_2O_3{\cdot}3CdO$ is the polymorph transformation at approximately 913 K, associated with a significant decrease in volume, resulting in the formation of an anion-deficient phase with a bcc structure (space group $I432$) [248, 251]. The crystal lattice of Bi_2CdO_4 is tetragonal (space group $I4_1/amd$), with infinite channels large enough for oxygen ion transfer [253].

The literature contains data on transport properties of Bi_2CuO_4 and solid solutions based on bismuth cuprate [18, 49, 238, 239, 240, 241, 242, 243], Bi_2PdO_4 [238], Bi_2O_3-ZnO and Bi_2O_3-CdO ceramics and single crystals [248, 253, 257, 258]. According to these results, the $Bi_2CuO_{4-\delta}$ phase in oxidizing conditions exhibits a predominant p-type electronic conductivity, which increases with increasing oxygen content in the oxide [18, 242, 246]. The oxygen ionic contribution to the total conductivity of bismuth cuprate becomes significant when the temperature increases up to 900–1000 K, but the oxygen ion transference numbers still do not exceed 0.05 [18, 239, 242]. The increasing role of ionic transport in $Bi_2CuO_{4-\delta}$ with increasing temperature correlates to oxygen losses, suggesting a vacancy mechanism for ionic conduction. Doping of bismuth cuprate with Ni, which leads to oxygen hyperstoichiometry, has no impact on ionic conductivity [242], unlike in the case of K_2NiF_4-type oxides such as $La_2CuO_{4+\delta}$ where increasing oxygen hyperstoichiometry results in a higher ionic transport due to oxygen interstitial migration [259, 260]. Figure 8 shows the temperature dependencies of the total conductivity of some Bi_2O_3-based electronic conductors, including $Bi_2CuO_{4-\delta}$. Owing to a high electrocatalytic activity, bismuth cuprate may be used as a sintering aid in the fabrication of $La(Sr)MnO_{3-\delta}$ electrode layers deposited onto zirconia-based solid electrolytes [241, 261, 262, 263]. Small additions of $Bi_2CuO_{4-\delta}$ to the manganite electrodes provided considerably low polarization resistances.

As for other sillenites and Bi_2MO_4 compounds, oxides of the Bi_2O_3-CdO and Bi_2O_3-ZnO systems also have significant ionic contributions to the total conductivity at temperatures above 900–1000 K [248, 253, 257]. For instance, the oxygen chemical diffusion coefficient of the high-temperature $Bi_{10}Cd_3O_{18-\delta}$ polymorph quenched down to 823 K, calculated from thermal gravimetry data, was 6×10^{-6} cm^2 s^{-1} [248]. The oxygen ionic conductivity of Bi_2CdO_4 increases with lower-valence cation doping, suggesting a vacancy mechanism for ion migration; the ion transference numbers of this phase at

Table 8 Transport properties of Bi_2SrO_4 calculated from the results on the total conductivity and e.m.f. [221]

Transport parameter	T (K)			Activation energy, E_a (kJ mol^{-1})
	1023 K	1073 K	1123 K	
Ionic conductivity, σ_o (S cm^{-1})	0.11	0.15	0.22	68.6
Electronic conductivity, σ_e (S cm^{-1})	0.067	0.076	0.085	21.2
Ion transference number, t_o	0.62	0.67	0.72	–

1020–1120 K vary in the range 0.5–0.8 [253]. In general, however, practical use of the Bi_2O_3-MO phases as mixed conductors seems to be unlikely owing to the relatively low ionic conductivity as well as numerous phase transitions.

Solid electrolytes and mixed conductors of Bi_2O_3-based multicomponent systems

As demonstrated in the previous reviews [1, 2, 3], the number of oxide phases in the ZrO_2-, HfO_2- and CeO_2-based systems is relatively small, and only a few of those are acceptable for electrochemical applications. Really, only solid solutions with the cubic fluorite-like structure, and several doped perovskite- and pyrochlore-type compounds based on zirconia, ceria and hafnia, may be considered for practical use. In contrast, bismuth oxide forms a variety of binary and ternary phases, as briefly listed above. However, while the applicability of a material requires an exact knowledge of, at least, partial ionic and electronic conductivities and stability under operating conditions, only a limited number of Bi_2O_3-based oxides have been properly characterized. For example, for many ternary and quaternary compounds of the aurivillius family, only the total conductivity was reported [89, 93]; however, these materials presumably possess a high ionic conduction at temperatures below 700 K. Owing to these constraints, only materials properly characterized are considered hereafter as solid electrolytes or mixed conductors. Among such materials, there are ternary and quaternary phases based on δ-Bi_2O_3 stabilized with REE or higher-valence metal oxides (δ*-Bi_2O_3) [18, 37, 38, 41, 42, 43, 44, 45, 46, 47, 53, 59, 102, 264, 265], γ-$Bi_4V_2O_{11}$ stabilized by partial substitution of vanadium with transition metals such as Cu or Ni (BIMEVOX) [48, 136, 137] and dual-phase mixed conductors consisting of a solid electrolyte phase (typically, δ*- or γ*-Bi_2O_3) and an electronically conducting phase like $BaBiO_{3-\delta}$, $Bi_2CuO_{4-\delta}$ or CoO_x [18, 37, 38, 45, 61, 62, 227, 246, 266, 267, 268, 269, 270]. The common trends for these multicomponent oxides may be summarized as follows:

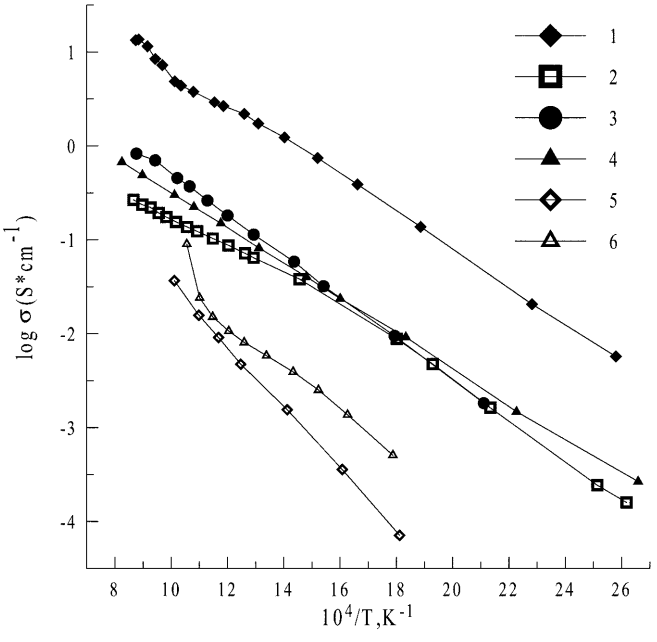

Fig. 8 Temperature dependence of the total conductivity of Bi_2O_3-based electronic conductors in air [230, 242]: *1*, $BaBiO_3$; *2*, $BaBi_{0.6}La_{0.4}O_3$; *3*, $BaBi_{0.6}Pr_{0.4}O_3$; *4*, $BaBi_{0.2}Pr_{0.8}O_3$; *5*, Bi_2CuO_4; *6*, $Bi_2Cu_{0.8}Ni_{0.2}O_4$

1. Incorporation of a third metal oxide into the ceramic composition has no effect on the stability of the Bi_2O_3-based materials with respect to reduction at low oxygen pressures. For example, no increase in the stability of Bi_2O_3-WO_3 solid solutions is observed when doping with REE oxides, Mg, Ca, Al or Pb [102]. Analogously, the stability limits of the solid solutions co-doped with different REE oxides are close to those characteristic of the Bi_2O_3-based systems containing one single dopant [18].
2. The thermal expansion of most Bi_2O_3-based phases is relatively high (Table 3), but decreases slightly with increasing dopant concentration. This tendency shows the correlation between thermal expansion and ionic conduction, which decreases with doping. For most well-known Bi_2O_3-based solid solutions, lowering of thermal expansion without reduction of ionic conductivity, by substitution of other metal cations for bismuth, is impossible. In the case of multiphase ceramics, thermal expansion is determined by the volume fractions and TECs of all phases present in the system.
3. Most of the known single-phase solid solutions based on bismuth oxide show p-type electronic conductivity in air. Doping of the Bi_2O_3-based phases with variable-valence cations such as Co, Mn or Pr leads, as a rule, to a greater electronic conduction. However, within the concentration limits of solid-solution formation, the variation of the electron transference numbers is relatively small, usually not exceeding 0.2. Only BIMEVOX phases doped with transition metals or praseodymium oxides show negligible changes in electronic conductivity ([136], Table 9). In this case, however, the solid solution formation concentration ranges are quite narrow.
4. As for binary systems, the ionic conductivity of ternary and quaternary solid solutions based on bismuth oxide exhibits a maximum for dopant concentrations close to the low stabilization limit and decreases with further substitution of bismuth. For dopant contents below the stabilization limit, the ionic conductivity is lower than the conductivity of completely stabilized phases at temperatures below the characteristic temperature of formation of ionically conducting phases; at higher temperatures the behavior is reversed.

5. As a general rule, segregation of secondary phases at grain boundaries of Bi_2O_3-based ceramics leads to decreasing ionic conductivity and increasing electronic transport. This is often associated with the blocking of ionic conduction at the grain boundaries and redistribution of the components between phases. For example, doping $Bi(Y)O_{1.5}$ solid solutions with BaO leads to formation of $BaBiO_{3-\delta}$ and, thus, to a decrease in bismuth content in the fluorite-type phase, which results in a lower ionic conductivity [18, 62, 227, 266].

Some of these features are observed also for the perovskite-related phases of the systems Bi-M^{II}-Co-O (M = Ca, Sr) [271, 272, 273, 274, 275] and $Ba(Bi, Ln)O_{3-\delta}$ (Ln = La, Pr) [229, 230], having predominant electronic conductivity. However, in this case the dependencies of the transport properties on composition are more complex. In particular, both ionic and electronic conductivities of $BaBi_{1-x}Ln_xO_{3-\delta}$ ($x = 0$–0.4) solid solutions decrease when bismuth is substituted by rare-earth cations [229]. At the same time, such substitution leads also to decreasing thermal expansion, which is similar to the behavior of other Bi_2O_3-based materials.

Fluorite-like ternary solid solutions

Within experimental error, single-phase solid solutions and multiphase ceramics in the ternary systems Bi_2O_3-Y_2O_3-ZrO_2 [41, 44, 46, 47, 59, 63], Bi_2O_3-Y_2O_3-La_2O_3 [18, 265], Bi_2O_3-Y_2O_3-BaO [18, 62, 227, 266, 267], Bi_2O_3-Y_2O_3-PbO [42, 43, 264], Bi_2O_3-Y_2O_3-CuO [18, 61, 246, 268], Bi_2O_3-Y_2O_3-CaF_2 [46, 47], Bi_2O_3-Ho_2O_3-Nb_2O_5 [41, 59], Bi_2O_3-Y_2O_3-PrO_x [44, 45, 47, 53] and Bi_2O_3-Y_2O_3-CoO_x [37, 38, 45, 200, 270] behave according to the above-mentioned trends. Analysis of data on ternary solid solutions shows that co-doping of Bi_2O_3 with two or more metal oxides may be useful to increase the conductivity and improve the material's phase stability. The increasing ionic transport is associated with the fact that the minimum dopant concentration necessary to stabilize the δ*-Bi_2O_3 phase is often lower in the ternary systems than in binary solid solutions. This results in a higher conductivity of compositions corresponding to the low stabilization limit, as observed for the solid solutions $Bi(Y, Zr)O_{1.5+\delta}$ [41, 44, 46], $Bi(La, Er)O_{1.5}$ [18, 265], $Bi(Nb, Ho)O_{1.5+\delta}$ [41] and $Bi(Y, Co)O_{1.5-\delta}$ [37, 38]. Table 10 lists the values of partial ionic and electronic conductivities of Bi_2O_3-Y_2O_3-CoO_x ceramics, showing the δ*-phase co-stabilization effect by yttrium and cobalt oxide additions.

A possible improvement in the stability of the fcc phase in the multicomponent systems could be achieved by suppressing the phase transformations, associated with cation diffusion, by introduction of higher-valence cations, such as Zr^{4+} or Th^{4+}, which decrease the interdiffusion coefficients [276]. However, the long-term stability tests of Bi_2O_3-Y_2O_3-ZrO_2 and Bi_2O_3-Ho_2O_3-Nb_2O_5 [41, 59] solid electrolytes demonstrated that the decomposition of the δ*-phase still takes place even at 873 K; additions of zirconia or niobia lead only to a lower rate of phase transformation. Zirconium dioxide is preferable as dopant (with respect to niobium pentoxide), as at 873 K no conductivity degradation was observed with time for Zr-doped materials (Fig. 9). It should be noted that degradation of the electrochemical cells may be caused also by interaction between Bi_2O_3-based ceramics and electrode layers [18, 59, 200], as illustrated in Fig. 9 for silver electrodes. These factors narrow the temperature applicability range of δ-Bi_2O_3-based solid solutions to approximately 900–950 K; the lower and upper limits are determined by the phase stability and interaction with electrodes, respectively.

Table 9 Oxygen ion transference numbers for $Bi_4V_2O_{11}$-based ceramics determined by the e.m.f. method under an oxygen partial pressure gradient of 1.0/0.21 atm [48]

Material	Phase composition[a]	T (K)	t_o
$Bi_2V_{0.90}Cu_{0.10}O_{5.5-\delta}$	γ	908	0.90
		850	0.98
		785	0.98
$Bi_{1.90}La_{0.10}V_{0.90}Cu_{0.10}O_{5.5-\delta}$	γ	908	0.92
		846	0.99
$Bi_{1.90}Pr_{0.10}V_{0.90}Cu_{0.10}O_{5.5-\delta}$	γ + I	908	0.94
		846	0.98

[a] γ and I correspond to the γ-$Bi_4V_2O_{11}$ phase and phase impurities, respectively

BIMEVOX-based ceramics

Solid solutions based on γ-$Bi_4V_2O_{11}$, stabilized down to room temperature by partial substitution of transition metal cations such as Cu and Ni for vanadium, exhibit superior ionic conductivity at temperatures below 800 K (Fig. 2); the oxygen ion transference numbers of such materials are close to unity (Table 9). Compared to the fluorite-like Bi_2O_3-based oxides, doped bismuth vanadate has an important advantage, namely the absence of phase decomposition at low temperatures. For instance, Fig. 10 shows that the conductivity of $Bi_2V_{0.9}Cu_{0.1}O_{5.5-\delta}$ (so-called BICUVOX.10) is independent of time at temperatures as low as 780 K. This might enable a significant reduction of operating temperatures of electrochemical cells such as oxygen pumps, resulting in considerable economic benefits. At the same time, practical use of bismuth vanadate-based ceramics for electrochemical applications is complicated owing to an extremely high chemical reactivity and low mechanical strength [48, 137]. Improvements in the chemical stability and strength of these materials can be obtained when bismuth is partially substituted with REE cations [48]; however, the solid solubility of lanthanum and praseodymium in the bismuth sublattice is low, preventing large changes in the properties of BIMEVOX phases [48, 136, 137]. In addition, the conductivity of

Table 10 Phase composition and partial ionic and electronic conductivities of $(Bi_{1-x}Co_x)_{1-y}Y_yO_{1.5-\delta}$ ceramics [270]

Cation composition		Phase composition[a]	Partial conductivities[b] at 1050 K	
x	y		σ_o (S cm^{-1})	σ_e (S cm^{-1})
0.10	0.10	$\delta+\gamma$	0.2	0.01
0.20	0.08	$\beta+\delta$	0.18	0.01
	0.10	$\delta+\gamma$	0.27	0.01
	0.11	δ	0.53	0.03
0.30	0.07	$\beta+\delta+$Co	–	–
	0.09	$\delta+\gamma+$Co	0.12	0.01
	0.10	δ	0.41	0.09
	0.14	$\delta+$Co	0.47	0.09
0.40	0.07	–	0.28	0.03
	0.10	$\delta+$Co	0.38	0.18
0.50	0.05	$\delta+\gamma+$Co	–	–
	0.07	$\delta+$Co	0.57	0.13
	0.09	$\delta+$Co	–	–
	0.10	$\delta+$Co	0.36	0.20
	0.12	$\delta+$Co	–	–
	0.14	$\delta+$Co	0.39	0.24
0.60	0.10	$\delta+$Co	0.31	0.25
	0.14	$\delta+$Co	–	–
0.70	0.10	$\delta+$Co	0.26	0.53
	0.12	$\delta+$Co	–	–
	0.14	$\delta+$Co	–	–

[a] β, γ, δ and Co correspond to the tetragonal β-, bcc γ- and fcc δ-phases of bismuth oxide and the Co_3O_4 phase, respectively
[b] The partial conductivities were calculated from the total conductivity and oxygen ion transference numbers determined by the e.m.f. method under an oxygen pressure gradient of 1.0/0.21 atm

BIMEVOX decreases with doping into both bismuth and vanadium sublattices. Comparative data on doped bismuth vanadate ceramics are given in Tables 3 and 7.

Weak mechanical properties are typical not only for doped γ-$Bi_4V_2O_{11}$ ceramics but also for most known Bi_2O_3-based materials, including fluorite-type solid solutions (e.g., [277]). Along with easy reduction at low oxygen pressures, this feature essentially limits the applicability in high-temperature electrochemical cells, usually having to face thermal shocks and mechanical stresses [9]. These problems might be solved using multilayer cells with a layer of Bi_2O_3-based ionic conductors applied on other materials, acting as mechanical support and protection against reduction. However, the high thermal expansion coefficients of bismuth oxide ceramics (Table 3) complicate this solution.

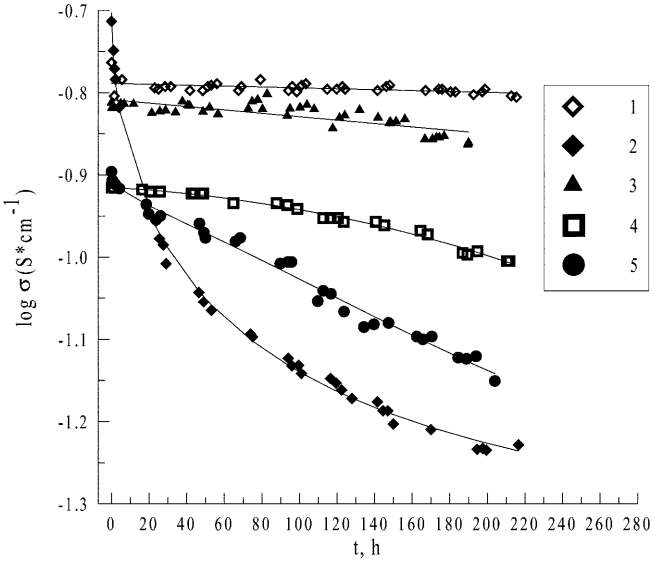

Fig. 9 Time dependence of the apparent electrical conductivity of $(Bi_{0.95}Zr_{0.05})_{0.85}Y_{0.15}O_{1.5+\delta}$ (*1*, *2*), $(Bi_{0.93}Zr_{0.07})_{0.85}Y_{0.15}O_{1.5+\delta}$ (*3*) and $(Bi_{0.95}Nb_{0.05})_{0.85}Ho_{0.15}O_{1.5+\delta}$ (*4*, *5*) at 873 K in air: *1* and *4*, Pt electrodes; *2* and *5*, Ag electrodes; *3*, electrodes of $La_{0.7}Sr_{0.3}CoO_{3-\delta}$ cobaltite. Data from [59] are used

Electrochemical properties and application tests of Bi_2O_3-based materials

Interaction with electrodes

The high chemical reactivity of Bi_2O_3-based ceramics results in numerous technological problems during fabrication of electrochemical cells and long-term operation. Most of these problems refer to interaction between electrolyte and electrode materials, leading to a perforation of bismuth oxide through the electrode, decreasing electrical conductivity and electrochemical activity of the electrode layers, and formation of diffusion layers between the electrode and electrolyte [38, 44, 46, 48, 59, 200, 277, 278, 279]. In addition, the electronic conductivity of the solid electrolyte might increase owing to diffusion of the electrode material. Silver electrodes were found unstable in contact with δ*-Bi_2O_3- and $Bi_4V_2O_{11}$-based ceramics [48, 59]. Layers of Pt exhibit a better stability (Figs. 9 and 10), but interaction with bismuth oxide is found also in the case of platinum [13, 18, 97, 170, 171, 280]. The reaction of Bi_2O_3-based electrolytes with perovskite-like cobaltites

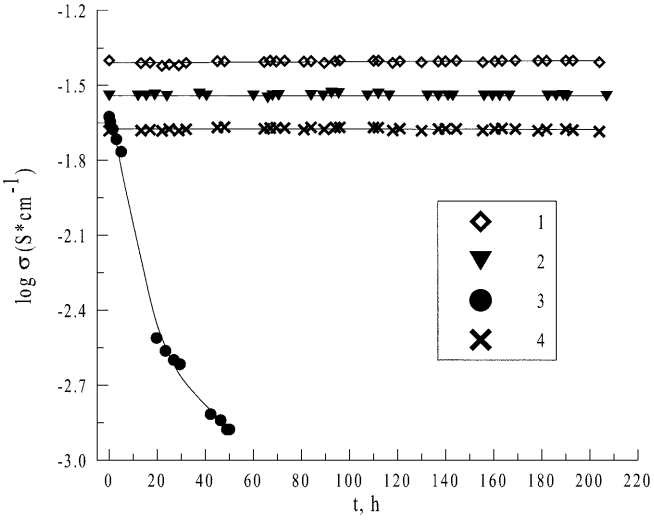

Fig. 10 Time dependence of the apparent electrical conductivity of $Bi_2V_{0.9}Cu_{0.1}O_{5.5-\delta}$ (*1*) and $Bi_{1.9}La_{0.1}V_{0.9}Cu_{0.1}O_{5.5-\delta}$ (*2–4*) at 780 K in air: *1* and *2*, Pt electrodes; *3*, Ag electrodes; *4*, electrodes of $La_{0.7}Sr_{0.3}CoO_{3-\delta}$. Data from [48] are used in the figure

of REE and strontium, which are promising electrode materials for electrochemical cells owing to high conductivity and electrochemical activity [38, 44, 278, 279, 281], occurs firstly in the course of electrode fabrication. Studies of diffusion layers between $Bi(Y)O_{1.5}$ and $La(Sr)CoO_{3-\delta}$ showed the formation of perovskite and fluorite solid solutions and cobalt oxide phases [38, 200]. In contrast with pyrochlore layers forming in cells with zirconia solid electrolytes and manganite electrodes [1, 2], the diffusion layers in cells with bismuth oxide could not be considered as completely blocking, since the phases formed possess significant mixed conductivity. At the same time, incorporation of bismuth into the perovskite phase leads to essentially worse oxygen transport (Table 11). Also, a decrease in ionic conductivity of the bismuth oxide ceramics takes place when the REE concentration increases or the cobalt oxide phase content becomes high (see [37, 38], Table 10). Thus, interdiffusion of Bi_2O_3-based electrolytes and cobaltite electrodes leads to worse oxygen transport through the electrode-electrolyte interface and electrical conduction along the electrode [46, 278, 279]; new electrodes or fabrication technologies are needed to avoid this detrimental interaction. As an example, Fig. 11 shows the temperature dependence of sheet resistance, normalized to the electrode thickness, for $La_{0.7}Sr_{0.3}CoO_{3-\delta}$ electrodes prepared by different techniques. The sheet resistance increases with annealing temperature but is a minimum for layers prepared by spraying nitrate solutions over heated solid-electrolyte substrates, when the interaction between materials is minimized [200, 278].

Interdiffusion of bismuth oxide electrolytes and lanthanum-strontium cobaltite and manganite electrodes takes place also in the course of operation of electrochemical cells, even at 970 K [277]. Decreasing operating temperatures are needed to suppress the interaction. As mentioned above, this behavior limits the possible use of δ*-Bi_2O_3-based electrolytes, since at temperatures below 870 K this phase becomes metastable.

Oxygen exchange of Bi_2O_3-based oxides

Isotopic oxygen exchange (OE) between bismuth oxide-based solid electrolytes and the gas phase was studied as a function of temperature, oxygen partial pressure and electrolyte composition [47, 284, 285, 286, 287, 288, 289, 290, 291, 292]. OE data on Bi-containing high-temperature superconductors have been reported [289, 293, 294]. Owing to the higher electronic conductivity of Bi_2O_3-based electrolytes, their oxygen exchange rates are 50–100 times higher than for stabilized zirconia (Fig. 12). Analogously, applying porous platinum layers onto the bismuth oxide ceramics has no significant effect on the OE rate, whereas the surface exchange of zirconia can be dramatically increased by deposition of layers of electronically conducting materials such as Pt, PrO_x or $La_{0.7}Sr_{0.3}CoO_{3-\delta}$ [289]. Comparison of exchange currents of the $Pt/Bi_{0.80}Er_{0.20}O_{1.5}$ system, measured by the isotopic

Table 11 Electrical conductivity and oxygen permeability of $La_{1-x}Bi_xCoO_{3-\delta}$ ceramics [200, 282, 283]

x	σ (S cm^{-1})	Specific oxygen permeability,[a] $J(O_2)$ (mol s^{-1} cm^{-1})		
	1115 K	1115 K	1175 K	1240 K
0	8.75×10^2	3.63×10^{-8}	4.07×10^{-8}	4.68×10^{-8}
0.05	8.91×10^2	0.62×10^{-8}	0.98×10^{-8}	1.35×10^{-8}
0.10	7.24×10^2	0.22×10^{-8}	0.28×10^{-8}	0.48×10^{-8}

[a] The values of the oxygen permeability are averaged in the oxygen partial pressure range 5×10^3 to 2.1×10^4 Pa

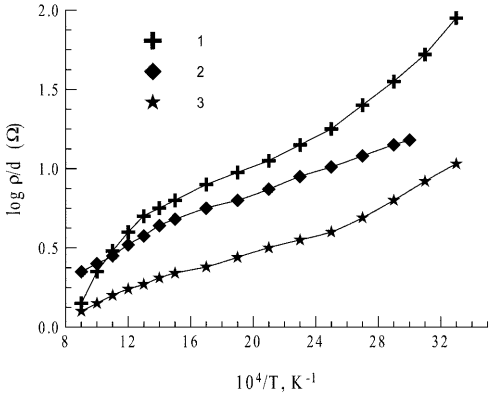

Fig. 11 Temperature dependence of the sheet resistance of $La_{0.7}Sr_{0.3}CoO_{3-\delta}$ electrodes (sheet density, 20–24 mg cm^{-2}), normalized to the electrode thickness (*d*), in air [38]. The electrodes were prepared on $Bi_{0.75}Y_{0.25}O_{1.5}$ substrates by firing of the powder at 1190 K (*1*), and by spraying of nitrate solution at 950–970 K (*2*) and 870–900 K (*3*)

method and calculated from polarization resistance measurements, demonstrated that only part of the oxygen is exchanged via electrochemical reactions over the electrode, clearly indicating a significant contribution of the electrolyte surface to the total OE rate [289]. Praseodymium oxide doping is responsible for increasing electronic conductivity [44, 45] but only slightly higher OE rates [287]; the opposite effect was observed for additions of ZrO_2 and CaF_2, which result in partial blocking of the electrolyte surface [47, 284]. In general, data on oxygen exchange suggests that electrode layers on Bi_2O_3-based solid electrolytes play mainly the role of current collectors, as opposed to the case of zirconia electrolytes where the OE kinetics is determined by the electrodes.

Detailed analysis of data on isotopic exchange kinetics of Bi_2O_3-based electrolytes (e.g., Fig. 13) showed that the OE rate is kept essentially constant when the depth of the bulk oxide participating in the OE processes increases up to 7–40% of the total oxygen content in the oxide bulk [287]. Such depths significantly exceed the oxygen monolayer thickness, showing that the bulk diffusion in Bi_2O_3-based ceramics is much faster than the surface exchange [286, 287]. This was confirmed also by estimates of oxygen self-diffusion rates, which are higher than the surface exchange rate by $\sim 10^9$ times at 973 K. Therefore, the limiting stage of the OE reaction in Bi_2O_3-based solid electrolytes is localized on the surface. Similar conclusions were obtained for Bi-containing superconducting phases [293].

For the fluorite-type solid solutions based on bismuth oxide, the dependence of oxygen exchange rate (R) on temperature and oxygen partial pressure can be adequately described by the equation [287]:

$$R = R_0 p_{O_2}^m \exp\left(-\frac{E_a}{RT}\right) \quad (7)$$

where m is the exchange reaction order, E_a is the activation energy and R_0 is the pre-exponential factor. The activation energy for the oxygen exchange of δ-Bi_2O_3-based electrolytes is in the range 115–176 kJ mol^{-1}; the reaction order is 0.92 and 0.7 for $Bi_{0.75}Y_{0.25}O_{1.5}$ and $Bi_{0.80}Er_{0.20}O_{1.5}$, respectively (Table 12). When analyzing the isotopic exchange types [295, 296], Kurumchin et al. [285, 287] found a prevailing exchange type III for stabilized δ-Bi_2O_3, involving two oxygen atoms of the oxide surface in the exchange reaction. Note that the reaction order, which varies between 0.5 (typical for the dissociative adsorption mechanism [285]) and 1.0, seems to be in agreement with such a conclusion.

Electrochemical properties of metal and oxide electrodes in contact with Bi_2O_3-based solid electrolytes

Electrode polarization in cells including metals (Ag, Pt), or perovskites such as $Ln(Sr)MeO_{3-\delta}$ (Me = Mn, Co) or $SrCo(Fe,Cu)O_{3-\delta}$ in contact with yttria- and erbia-stabilized Bi_2O_3-based electrolytes, has been addressed [18, 37, 38, 44, 46, 47, 200, 277, 278, 279, 284, 297]. Data on double-layer electrode systems consisting of metallic layers deposited onto underlayers of mixed conductors, including $BaBiO_{3-\delta}$ [18, 227], $(Bi_{0.3}Co_{0.7})_{0.9}Y_{0.1}O_{1.5}$

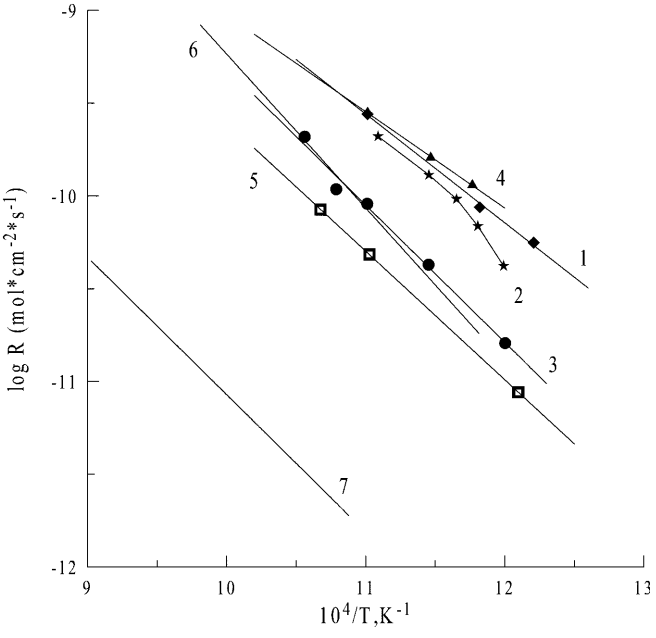

Fig. 12 Temperature dependence of the interphase oxygen exchange rate at an oxygen partial pressure of 1.33×10^3 Pa [47, 284, 287]: *1*, $Bi_{0.75}Y_{0.25}O_{1.5}$; *2*, $(Bi_{0.75}Y_{0.25}O_{1.5})_{0.95}(ZrO_2)_{0.05}$; *3*, $(Bi_{0.75}Y_{0.25}O_{1.5})_{0.70}(ZrO_2)_{0.30}$; *4*, $(Bi_{0.75}Y_{0.25}O_{1.5})_{0.95}(PrO_{1.833})_{0.05}$; *5*, $(Bi_{0.75}Y_{0.25}O_{1.5})_{0.96}(CaF_2)_{0.04}$; *6*, $Bi_{0.80}Er_{0.20}O_{1.5}$; *7*, $Zr_{0.9}Y_{0.1}O_{1.95}$

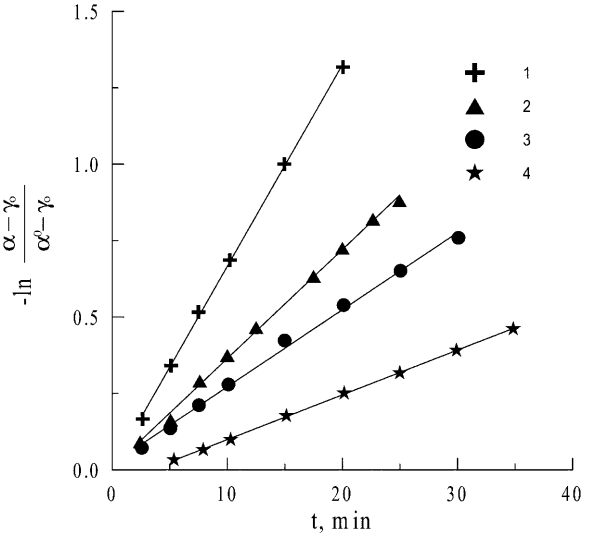

Fig. 13 Oxygen isotopic exchange kinetics of the $Bi_{0.75}Y_{0.25}O_{1.5}$ solid electrolyte [$p(O_2) = 1.33\times10^3$ Pa] at 908 K (*1*), 873 K (*2*), 845 K (*3*) and 822 K (*4*), where α is the ^{18}O isotope concentration in the gas phase, α^0 is the starting value of α, and γ_o is the isotope concentration at equilibrium between the oxide and gas phase. Data from [287] are used in the figure

Table 12 Parameters for oxygen exchange between Bi_2O_3-based oxides and the gas phase

Composition	Specific surface area ($m^2\ g^{-1}$)	Activation energy for oxygen exchange, E_a (kJ mol^{-1})	Reaction order, m	Ref.
$Bi_{0.75}Y_{0.25}O_{1.5}$	0.28	115	0.92	[287]
$(Bi_{0.75}Y_{0.25}O_{1.5})_{0.95}(ZrO_2)_{0.05}$	0.16	161	–	[287]
$(Bi_{0.75}Y_{0.25}O_{1.5})_{0.70}(ZrO_2)_{0.30}$	0.03	157	–	[287]
$(Bi_{0.75}Y_{0.25}O_{1.5})_{0.96}(CaF_2)_{0.04}$	0.20	135	–	[287]
$(Bi_{0.75}Y_{0.25}O_{1.5})_{0.95}(PrO_{1.833})_{0.05}$	0.77	115	–	[287]
Bi_2O_3	0.26	200	–	[287]
Bi_2O_3	0.20	172	0.6	[291]
$Bi_{0.80}Er_{0.20}O_{1.5}$	0.07	176	0.7	[285]
$Bi_{0.80}Er_{0.20}O_{1.5}$/Pt	–	159	0.7	[288]

[37, 200], Bi_2CuO_4 [18, 246], $Bi_{0.8}Tb_{0.2}O_{1.5+\delta}$ and $(Bi_{0.75}Y_{0.25}O_{1.5})_{0.95}(PrO_{1.833})_{0.05}$ [44, 46, 47], is also available. The trends observed in most data may be summarized as follows. Firstly, interaction of electrodes with the solid electrolyte leads to decreasing electrochemical activity (e.g., [46, 200, 277, 279]). In the case of oxide electrode layers, this is associated with a partial phase decomposition of both electrode and electrolyte, and with a decrease in ionic conductivity of the solid electrolyte surface layer owing to diffusion of rare-earth and/or alkaline-earth cations [38, 200]. For metal electrodes, probable reasons for the increasing polarization resistance are metal dissolution in the bulk electrolyte and penetration of bismuth oxide into the electrode surface, blocking the active zones. Secondly, no direct correlation is observed between electrochemical activity of oxide electrodes and partial electronic and ionic conductivities of the electrode materials [38, 44, 46, 200]. This feature is clear, taking into account the data on oxygen exchange, showing a high surface activity of Bi_2O_3-based solid electrolytes. As a consequence, deposition of mixed-conducting underlayers between electrode and electrolyte has no effect on the polarization resistance [44, 46, 47]. Thirdly, electrocatalytic and transport properties of oxide electrodes and, probably, of the surface layers of bismuth oxide electrolytes depend on the applied overpotential (η). As a particular result, usually the classical Butler-Volmer equation is not observed, and establishing simple relationships between the polarization at low and high overpotentials is complicated. For example, the lowest polarization resistance ($|\eta| < 10$ mV) with respect to other REE and strontium cobaltites was found for the composition $La_{0.7}Sr_{0.3}CoO_{3-\delta}$, whereas at higher overpotentials ($|\eta| > 40$ mV) the minimum polarization was found for $Nd_{0.5}Sr_{0.5}CoO_{3-\delta}$ [38, 200, 278]. Notice that the neodymium-strontium cobaltite has significantly lower ionic conductivity than $La(Sr)CoO_{3-\delta}$ and $Pr(Sr)CoO_{3-\delta}$, while the electronic conductivities of these cobaltites are similar [281, 298]; the high electrochemical activity of $Nd_{0.5}Sr_{0.5}CoO_{3-\delta}$ should be attributed, hence, to specific electrocatalytic activity [46].

Cermet electrode layers consisting of $Nd_{0.5}$ $Sr_{0.5}$ $CoO_{3-\delta}$ and metallic silver demonstrated good performance (Fig. 14). For instance, using these cermet electrodes, current densities as high as 1.2 A cm^{-2} can be reached without decomposition of the $Bi(Y)O_{1.5}$ solid electrolyte, whilst the maximum currents for the cobaltite electrodes were about 0.5 A cm^{-2} [44, 277]. However, Ag-containing electrode layers are hardly acceptable owing to melting of silver at moderate overpotentials, caused by dissolution of oxygen [299, 300], and interaction of Ag with Bi_2O_3-based electrolytes [59].

For most metal and oxide electrodes in contact with stabilized bismuth oxide, the polarization resistance (R_η) as a function of oxygen partial pressure in the range 1 Pa to 2.1×10^5 Pa and temperature 670–970 K can be adequately described by Eq. 8, similar to Eq. 7 [46, 47, 200, 278, 279, 284]:

$$R_\eta = A_0 T p_{O_2}^{-m} \exp\left(\frac{E_a}{RT}\right) \quad (8)$$

where A_0 is the pre-exponential factor. Table 13 lists the regression parameters obtained for the cathodic polarization resistance of various electrodes applied on $Bi_{0.75}Y_{0.25}O_{1.5}$ solid electrolytes. Similar data on silver electrodes in contact with different electrolytes are given in Table 14. As a rule, the regression parameters (Eq. 8) for anodic and cathodic polarization are close to each other, within the experimental error limits [44, 46, 47, 200, 278, 279]. Table 13 presents data on both anodic and cathodic regimes for silver electrodes.

Finally, one should mention the attempts to use sintering aids, such as CuO [277], or to incorporate copper into the crystal lattice of $Sr(Co,Fe)O_{3-\delta}$ perovskites [46, 279, 301, 302] in order to decrease the annealing temperature of the electrodes and, thus, to suppress their interaction with the electrolyte, in the course of fabrication. However, doping with copper was found to decrease the electrochemical activity of strontium cobaltites-ferrites [46, 279], which may be caused either by formation of the Bi_2CuO_4 phase, blocking ionic transport through the electrode-electrolyte interface, or by abatement of the Cu-doped perovskites' ionic and electronic conductivities [301, 302].

Response of potentiometric oxygen sensors composed of Bi_2O_3-based electrolytes

The dynamic characteristics of potentiometric oxygen sensors based on $Bi_{1-x}Y_xO_{1.5}$ ($x = 0.25$–0.50), ($Bi_{0.75}$

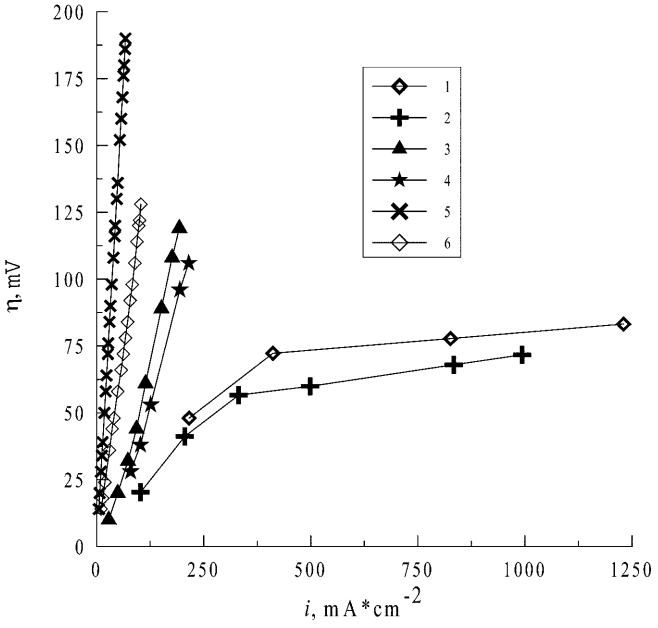

Fig. 14 Dependencies of overpotential on current density in atmospheric air: *1* and *2*, anodic and cathodic polarization of Ag-$Nd_{0.5}Sr_{0.5}CoO_{3-\delta}$ cermet electrode at 950 K, respectively [44]; *3* and *4*, anodic and cathodic polarization of $Nd_{0.5}Sr_{0.5}CoO_{3-\delta}$ electrode at 950 K, respectively [44]; *5* and *6*, anodic polarization of $La_{0.7}Sr_{0.3}CoO_{3-\delta}$ and $SrCo_{0.5}Fe_{0.5}O_{3-\delta}$ electrodes at 910 K, respectively [46]. The solid electrolyte is $Bi_{0.76}Zr_{0.04}Y_{0.20}O_{1.52}$ (curves *1* and *2*) and $Bi_{0.75}Y_{0.25}O_{1.5}$ (*3–6*). Absolute values of the overpotential are given for convenience

$Y_{0.25}O_{1.5})_{1-x}(CaF_2)_x$ ($x = 0.01$–0.05) and $(Bi_{0.75}Y_{0.25}O_{1.5})_{0.95}(ZrO_2)_{0.05}$ solid electrolytes were tested under conditions of step-type changes in oxygen partial pressure corresponding to "air↔oxygen" and "air↔nitrogen" switching [46, 47, 200, 278]. In order to calculate the transient parameters, including the 95% response time ($t_{0.95}$), a polynomial approximation of the sensor e.m.f. was proposed [47]:

$$E(\xi) = B_0 + \sum_{i=2}^{n} B_i \xi^i \qquad (9)$$

where ξ is the transformed variable defined as $\xi = \exp(-t/\tau)$, t is the time elapsed after the experiment started, τ is the time required to reach approximately 90% of the final signal, and n is the polynomial degree necessary to fit the experimental response to Eq. 9 (as a rule, $n = 4$ or 5). The transient processes revealed the following aspects [46, 47]:

1. The response on decreasing the oxygen partial pressure is significantly slower than when the oxygen pressure increases. This may be explained, in particular, in terms of simple adsorption-desorption models, where the oxygen sorption rate is proportional to the oxygen pressure multiplied by the surface concentration of unoccupied sites [46, 47].
2. The response time decreases with increasing gas flow rate. This behavior, found for all tested sensors, is due to the oxygen transport limitations in the gas phase. Increasing flow rates lead to a decreasing role of this factor, and the sensor response rates approach their asymptotic values [47].
3. The response characteristics of the potentiometric cells are not directly related to the transport and elecrochemical properties of sensor materials such as the conductivity of the solid electrolyte, polarization resistance of the electrodes or oxygen exchange rates [47]. The observed trends may be only qualitatively explained in terms of the specific catalytic activity of the electrode and electrolyte materials. For instance, additions of 4 mol% CaF_2 to $Bi_{0.75}Y_{0.25}O_{1.5}$ lead to a considerable decrease in response time, which was attributed to formation of calcium fluoride microcrystals at the grain boundaries of the ceramic electrolyte, acting as catalytic sites [46, 47].

Also, chemisorption and bulk oxygen exchange of the electrodes result, as a rule, in greater response times. As an example, the dynamic characteristics of a sensor with a $La_{0.7}Sr_{0.3}CoO_{3-\delta}$ measuring electrode, where relatively slow bulk oxygen exchange takes place with oxygen

Table 13 Cathodic polarization characteristics of different electrodes in contact with $Bi_{0.75}Y_{0.25}O_{1.5}$ electrolyte [46, 47, 200]

Electrode	Preparation method[a]	$\ln(A_0)$	m	E_a (kJ mol^{-1})
Ag	A	-23.1 ± 0.7	0.41 ± 0.02	147 ± 5
Ag (anodic polarization)	A	-23.2 ± 0.4	0.44 ± 0.01	150 ± 3
Pt	A	-25 ± 2	0.18 ± 0.04	165 ± 15
$(Bi_{0.75}Y_{0.25}O_{1.5})_{0.98}(PrO_{1.833})_{0.02}$	A	-20.4 ± 0.1	0.375 ± 0.005	127 ± 1
$(Bi_{0.75}Y_{0.25}O_{1.5})_{0.95}(PrO_{1.833})_{0.05}$	A	-20.3 ± 0.3	0.23 ± 0.01	124 ± 2
$B_{0.8}Tb_{0.2}O_{1.5}$	A	-18.9 ± 0.3	0.35 ± 0.01	117 ± 2
$La_{0.7}Sr_{0.3}CoO_3$	S	-19.8 ± 0.4	0.37 ± 0.01	114 ± 3
$Pr_{0.5}Sr_{0.5}CoO_3$	S	-11.6 ± 0.4	0.61 ± 0.02	79 ± 3
$Nd_{0.5}Sr_{0.5}CoO_3$	S	-13 ± 2	0.57 ± 0.09	75 ± 9
$SrCo_{0.5}Fe_{0.5}O_3$	S	-16.5 ± 0.7	0.35 ± 0.03	99 ± 5
$SrCo_{0.6}Fe_{0.2}Cu_{0.2}O_3$	S	-22.1 ± 1	0.23 ± 0.03	122 ± 9
$SrCo_{0.6}Fe_{0.2}Cu_{0.2}O_3$	A	-22.4 ± 0.9	0.26 ± 0.04	130 ± 7
$SrCo_{0.5}Fe_{0.3}Cu_{0.2}O_3$	S	-20 ± 1	0.16 ± 0.03	132 ± 9
$Bi_{0.27}Co_{0.63}Y_{0.10}O_{1.5}$	S	-19.5 ± 0.5	0.29 ± 0.01	131 ± 3

[a] A corresponds to annealing a layer, deposited using a paste of highly dispersed powder and organic binder; S refers to spraying the nitrate solution over the heated solid-electrolyte substrate

Table 14 Cathodic polarization characteristics of silver electrodes in contact with different Bi_2O_3-based solid electrolytes [46, 47]

Electrolyte	$\ln(A_0)$	m	E_a (kJ mol^{-1})
$(Bi_{0.95}Z_{0.05}O_{1.525})_{0.85}(YO_{1.5})_{0.15}$	-16.8 ± 0.4	0.31 ± 0.01	101 ± 2
$(Bi_{0.95}Z_{0.05}O_{1.525})_{0.80}(YO_{1.5})_{0.20}$	-15.7 ± 0.4	0.33 ± 0.02	93 ± 3
$(Bi_{0.90}Z_{0.10}O_{1.55})_{0.85}(YO_{1.5})_{0.15}$	-19.6 ± 0.3	0.30 ± 0.01	118 ± 2
$(Bi_{0.75}Y_{0.25}O_{1.5})_{0.95}(ZrO_2)_{0.05}$	-15.1 ± 0.6	0.32 ± 0.02	87 ± 4
$(Bi_{0.75}Y_{0.25}O_{1.5})_{0.99}(CaF_2)_{0.01}$	-13.5 ± 1	0.35 ± 0.03	76 ± 7
$(Bi_{0.75}Y_{0.25}O_{1.5})_{0.98}(CaF_2)_{0.02}$	-16.1 ± 0.2	0.31 ± 0.01	96 ± 1
$(Bi_{0.75}Y_{0.25}O_{1.5})_{0.97}(CaF_2)_{0.03}$	-21.9 ± 0.6	0.29 ± 0.02	137 ± 3
$(Bi_{0.75}Y_{0.25}O_{1.5})_{0.96}(CaF_2)_{0.04}$	-21.2 ± 0.4	0.34 ± 0.01	131 ± 3
$(Bi_{0.75}Y_{0.25}O_{1.5})_{0.95}(CaF_2)_{0.05}$	-19.3 ± 0.9	0.30 ± 0.01	114 ± 6

pressure changes, are considerably worse than those for silver electrodes (Fig. 15). At the same time, deposition of sublayers of mixed conductors, such as $Bi_{0.8}Tb_{0.2}O_{1.5+\delta}$, between the electrolyte and electrode has often no significant effect on the response parameters [47]. In this section, one should also mention results [303] showing that the response rate of potentiometric sensors can be improved by applying an a.c. voltage (5–6 V) to the electrodes.

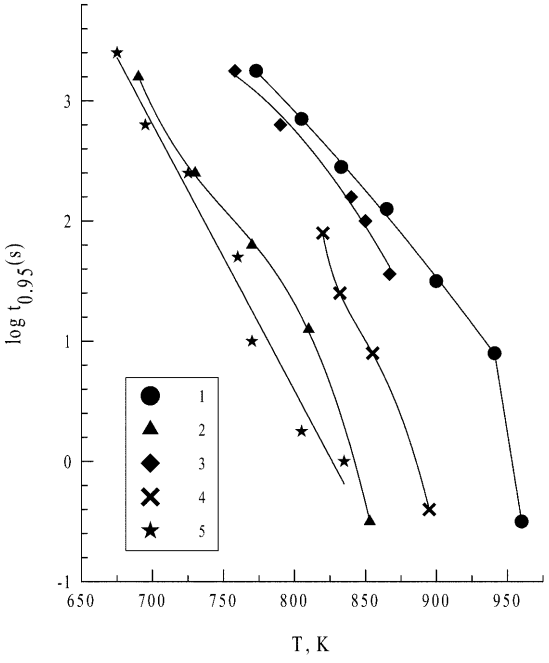

Fig. 15 Temperature dependence of the 95% response time at "air→oxygen" switching for the potentiometric sensors with the solid electrolytes $Bi_{0.75}Y_{0.25}O_{1.5}$ (*1–3*), $(Bi_{0.75}Y_{0.25}O_{1.5})_{0.95}(ZrO_2)_{0.05}$ (*4*) and $(Bi_{0.75}Y_{0.25}O_{1.5})_{0.96}(CaF_2)_{0.04}$ (*5*). The measuring electrodes are from Pt (curve *1*), Ag (*2*, *4* and *5*) or $La_{0.7}Sr_{0.3}CoO_{3-\delta}$ (*3*). Data from [46, 47, 200] are used

Application tests

Neglecting the above-mentioned disadvantages of Bi_2O_3-based electrolytes, a number of research projects was performed to test these materials for practical applications, including oxygen pumps [44, 304] and oxygen potentiometric sensors [47, 305]. For miniaturized oxygen sensors with reduced energy consumption, the construction with a hermetically sealed reference electrode (Fig. 16a) was chosen [305]. Such a choice was based on the advantages of Bi_2O_3-based solid electrolytes, particularly a higher conductivity than that of stabilized zirconia at moderate temperatures [305]; when the energy consumption is not extremely limited, zirconia can be used with obvious advantage. Metal-oxide reference electrodes such as Cu/Cu_2O, Cu_2O/CuO, Bi/Bi_2O_3 and Pd/PdO demonstrated excessively prolonged equilibration processes in the heating-cooling cycles. The best reference electrodes were SrCo(Fe)$O_{3-\delta}$ solid solutions [305], whose properties have been reported in detail [306]. The temperature range for the sensor operation was 783–833 K; the response as a function of oxygen chemical potential was linear down to oxygen concentrations in the gas phase of about 10^{-5} vol% [305]. The chosen design provided reasonable technical characteristics (weight of 2 g, resistance of approximately 100 Ω).

Another interesting development refers to an oxygen pump developed recently at the Institute of High-Temperature Electrochemistry of the Russian Academy of Science [304]. A schematic drawing of the cross-section of this pump is given in Fig. 16b. Such a cell was reported to provide an average oxygen flux of 5.2 L h^{-1} with a Faradaic efficiency higher than 95% [304].

Final comments

Oxygen ion-conducting materials based on Bi_2O_3 have limited use for high-temperature electrochemical applications owing to high reactivity, volatilization of bismuth oxide, easy reducibility at low oxygen pressures, low mechanical strength and high thermal expansion. In addition, the stabilized δ-Bi_2O_3 fluorite-type phases decompose at temperatures below 870 K. The present level of knowledge on effects of doping provides no direction to suppress these disadvantages. The only obvious way to improve the applicability of bismuth oxide phases might be reducing the electrochemical cell's operating temperature. This holds for materials exhibiting no phase transformation down to room temperature, such as, probably, the BIMEVOX series, but not to δ-Bi_2O_3-

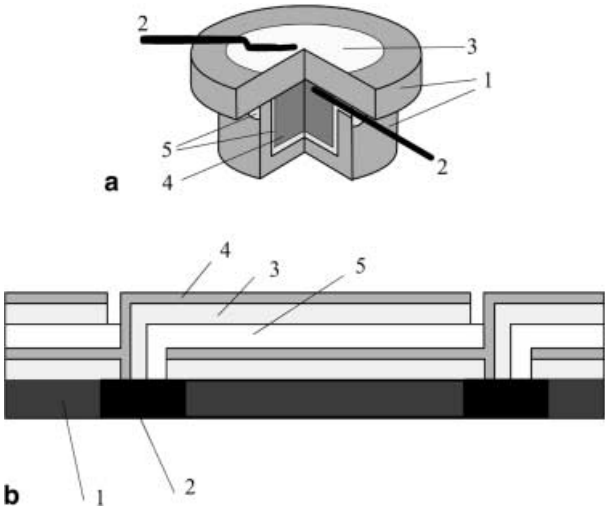

Fig. 16a, b Schematic drawing of sample cells with bismuth oxide-based ceramics. a Potentiometric oxygen sensor: *1*, $Bi_{0.75}Y_{0.25}O_{1.5}$ electrolyte; *2*, silver current collectors; *3*, silver measuring electrode; *4*, reference electrode; *5*, glass sealant. b Cross section of the oxygen pump wall: *1* and *2*, porous and dense parts of the support; *3*, lanthanum-strontium manganite; *4*, chromium carbide, Cr_3C_2; *5*, Bi_2O_3-based solid electrolyte

based solid solutions, metastable at low temperatures. While fluorite-type oxides have been extensively studied, many aurivillius-type compounds, which might be more promising from a viewpoint of moderate temperature applications, are not yet properly characterized. There is thus a clear contradiction between the present level of knowledge and the potential of these materials for further developments. On the other hand, one should notice that lowering the operational temperatures of electrochemical cells is also limited by an exponential increase of electrode polarization resistance with decreasing temperature; novel electrode materials with higher electrochemical activity are needed for this purpose. New electrochemical cell concepts compatible with the utilization of these electrolyte materials under increasing applied voltages, or under large oxygen chemical potential gradients, are also needed to improve their applicability domain. The interest in Bi_2O_3-based ionic conductors, considered in this review, is now rather more academic than practical. However, the high oxygen ionic conductivity of many bismuth oxide phases is a serious driving force to look for solutions for these problems in the future.

References

1. Kharton VV, Naumovich EN, Vecher AA (1999) J Solid State Electrochem 3:61
2. Kharton VV, Yaremchenko AA, Naumovich EN (1999) J Solid State Electrochem 3:303
3. Kharton VV, Yaremchenko AA, Naumovich EN, Marques FMB (2000) J Solid State Electrochem 4:243
4. Zhuk PP, Samokhval VV (1986) Ionn Raspl Tverd Elektrolity (Ionic Melts and Solid Electrolytes) (1):80
5. Zhuk PP, Vecher AA, Samokhval VV (1984) Vestn Belarus Univ Ser 2 (1):8
6. Shuk P, Wiemhofer H-D, Guth U, Gopel W, Greenblatt M (1996) Solid State Ionics 89:179
7. Sammes NM, Tompsett GA, Nafe H, Aldinger F (1999) J Eur Ceram Soc 19:1801
8. Chebotin VN, Perfilyev MV (1978) Electrochemistry of solid electrolytes (in Russian). Khimiya, Moscow
9. Perfilyev MV, Demin AK, Kuzin BL, Lipilin AS (1988) High-temperature electrolysis of gases (in Russian). Nauka, Moscow
10. Murygin IV (1991) Electrode processes in solid electrolytes (in Russian). Nauka, Moscow
11. Samokhval VV, Kharton VV, Naumovich EN, Vecher AA (1994) Methods to investigate transport of charge particles in oxide materials. Textbook for students (in Russian). Belarus State University, Minsk
12. Toropov NA, Barzakovskii VP, Lapin VV, Kurtseva NN (1969) Phase diagrams of silicate systems. A handbook, vol 1 (in Russian). Nauka, Leningrad
13. Skorikov VM, Kargin YuF (1988) Chemistry of bismuth oxide compounds. In: Studies on inorganic chemistry and chemical technology (in Russian). Nauka, Moscow, pp 261–278
14. Zavyalova AA, Imamov RM, Pinsker ZG (1964) Kristallografiya 9:857
15. Zavyalova AA, Imamov RM (1972) Zh Strukt Khim 13:869
16. Zosimovich DP, Tsimmergakl VA (1949) Ukr Khim Zh 15:351
17. Reznitsky LA (1990) Zh Fiz Khim 64:1669
18. Poluyan AF (1987) PhD Thesis, Belarus State University, Minsk
19. Fomchenkov LP, Mayer AA, Gracheva NA (1974) Neorg Mater 10:2020
20. Korobeinikova AV, Kholmov VA, Reznitsky LA (1976) Vestn Moskov Univ Ser 2 17:381
21. Batog VN, Pakhomov VI, Safronov GM, Fedorov PM (1973) Neorg Mater 9:1576
22. Zavyalova AA, Imamov RM (1969) Kristallografiya 14:331
23. Zavyalova AA, Imamov RM (1971) Kristallografiya 16:516
24. Zavyalova AA, Imamov RM, Pinsker ZG (1965) Kristallografiya 10:480
25. Zavyalova AA, Imamov RM (1968) Kristallografiya 13:49
26. Sillen LG (1937) Arkiv Kemi Mineral Geol 12A:1
27. Semiletov SA, Pinsker ZG (1955) Zh Tekhn Fiz 25:13
28. Agasiev AA, Zeinally AKh, Alekperov SJ, Guseinov YaYu (1986) Mater Res Bull 21:765
29. Shuk P, Möbius H-H (1985) Z Phys Chem 266:9
30. Konovalov VM, Kulakov VI, Fidrya AK (1955) Zh Tekh Fiz 25:1864
31. Zolyan TS, Regel AR (1963) Fiz Tverd Tela 5:2420
32. Poznyak SK, Kulak AI (1984) Elektrokhimiya 20:1531
33. Poznyak SK, Kulak AI (1984) Elektrokhimiya 20:1393
34. Ikonopisov S, Klein E, Andreeva L, Nikolow Ts (1974) Thin Solid Films 11:22
35. Chebotin VN (1982) Physical chemistry of solids (in Russian). Khimiya, Moscow
36. Poluyan AF, Vecher AA, Samokhval VV, Savitsky AA (1984) Vestn Belarus Univ Ser 2 (2):5
37. Kharton VV, Naumovich EN, Zhuk PP, Tonoyan AA, Vecher AA (1992) Vesti Akad Nauk Belarusi Ser Khim (2):35
38. Kharton VV, Naumovich EN, Samokhval VV (1997) Solid State Ionics 99:269
39. Gilderman VK, Palguev SF, Dal AG (1988) Electrochemical properties of $(Bi_2O_3)_{0.8}(Er_2O_3)_{0.2}$ and $(Bi_2O_3)_{0.75}(Er_2O_3)_{0.15}$ solid electrolytes. In: Solid state chemistry (in Russian). Academy of Sciences of the USSR, Ural Dept., Sverdlovsk, pp 28–33
40. Yaremchenko AA, Kharton VV, Naumovich EN, Vecher AA (1998) J Solid State Electrochem 2:146

41. Yaremchenko AA, Kharton VV, Naumovich EN, Tonoyan AA, Samokhval VV (1998) J Solid State Electrochem 2:308
42. Naumovich EN, Skilkov SA, Kharton VV, Tonoyan AA, Vecher AA (1994) Russ J Electrochem 30:642
43. Naumovich EN, Kharton VV, Skilkov SA, Samokhval VV (1995) Inorg Mater 31:1329
44. Naumovich EN, Kharton VV, Samokhval VV, Kovalevsky AV (1997) Solid State Ionics 93:95
45. Naumovich EN, Kharton VV, Kovalevsky AV, Samokhval VV (1998) In: Ramanarayanan TA (ed) Ionic and mixed conducting ceramics. III. The Electrochemical Society, Pennington, pp 496–508
46. Kharton VV, Naumovich EN (1993) Russ J Electrochem 29:1297
47. Naumovich EN (1991) PhD Thesis, Belarus State University, Minsk
48. Yaremchenko AA, Kharton VV, Naumovich EN, Marques FMB (2000) J Electroceram 4:235
49. Tikhonova LA, Kononyuk IF, Zonov YuG, Makhnach LV (1990) Neorg Mater 26:1495
50. Vasilyeva IA, Mayorova AF (1985) Dokl Akad Nauk SSSR 280:385
51. Berezovskaya YuM, Vasilyeva IA, Mayorova AF (1988) Dokl Akad Nauk SSSR 301:626
52. Takahashi T, Iwahara H, Arao T (1975) J Appl Electrochem 5:187
53. Zhuk PP, Naumovich EN, Vecher AA, Bumblis AM (1990) Ionn Raspl Tverd Elektrolity (Ionic Melts and Solid Electrolytes) (5):77
54. Poluyan AF, Voropaev AG, Vecher AA (1986) In: 37th meeting, International Society of Electrochemistry, ext abstr, vol 3. VINITI, Lubertsy, pp 36–38
55. Berezovskaya YuM, Vasilyeva IA, Mayorova AF (1989) Zh Fiz Khim 63:611
56. Watanabe A (1996) Solid State Ionics 86–88:1427
57. Kruidhof H, de Vries KJ, Burggraaf AJ (1990) Solid State Ionics 37:213
58. Kruidhof H, Bouwmeester HJM, de Vries KJ, Gellings PJ, Burggraaf AJ (1992) Solid State Ionics 50:181
59. Yaremchenko AA, Kharton VV, Naumovich EN, Tonoyan AA (2000) Mater Res Bull (in press)
60. Neuimin AD, Yushina LD, Ovchinnikov YuM, Palguev SF (1963) Trudy Inst Elektrokhim (4):111
61. Poluyan AF, Gusakov AG (1987) Ionn Raspl Tverd Elektrolity (Ionic Melts and Solid Electrolytes) (2):78
62. Poluyan AF, Zhuk PP, Vecher AA, Samokhval VV (1988) Vesti Akad Nauk BSSR Ser Khim (2):58
63. Vecher AA, Zhuk PP, Naumovich EN, Khodorenko TG (1989) Ionn Raspl Tverd Elektrolity (Ionic Melts and Solid Electrolytes) (4):73
64. Vasilyeva IA, Shaulova EYu, Sukhushina IS, Shehtman SN (1971) Zh Fiz Khim 45:2013
65. Gorelov VP (1988) Elektrokhimiya 24:1380
66. Belkova TB, Neyman AYa, Konisheva EYu (1997) Neorg Mater 33:988
67. Neyman AYa, Belkova TB (1997) Elektrokhimiya 33:1082
68. Belkova TB, Vovkotrub EG, Neyman AYa (1994) Zh Neorg Khim 39:219
69. Aleksandrov VI, Osiko VV, Prokhorov NM, Tatarintsev VM (1978) Usp Khim 47:385
70. Novikov GI, Leonovich IB, Strugach LS, Rudakov VV (1985) Vesti Akad Nauk BSSR Ser Khim (3):3
71. Yanovsky VK, Voronkova VI, Aleksandrovsky AL, Dyakov VA (1975) Dokl Akad Nauk SSSR 222:94
72. Yanovsky VK, Voronkova VI, Roginskaya YuE, Venevtsev YuN (1982) Fiz Tverd Tela 24:2829
73. Shuvaeva ET, Fesenko EG (1980) Kristallografiya 25:408
74. Leonov AI, Voronkova VI, Stefanovich SYu, Shifrina RR, Yanovsky VK (1986) Zh Neorg Khim 31:3110
75. Yanovsky VK, Voronkova VI, Milyutin VA (1983) Kristallografiya 28:316
76. Speranskaya EI (1970) Neorg Mater 6:149
77. Smolyaninov NP, Belyaev IN (1962) Zh Neorg Khim 7:2591
78. Galperin EL, Erman LYa, Kolchin IK, Belova MA, Chernishev KS (1966) Zh Neorg Khim 11:2125
79. Osipyan VG, Shebanov LA, Freidenfeld EZh (1983) Zh Neorg Khim 28:728
80. Yanovsky VK, Voronkova VI, Lukhina VN (1986) Neorg Mater 22:1199
81. Roginskaya YuE, Utkin VI, Shifrina RR, Galyamov BSh, Venevtsev YuN (1982) Zh Fiz Khim 56:3034
82. Utkin VI, Roginskaya YuE, Kayumov RP, Venevtsev YuN (1980) Zh Fiz Khim 54:2953
83. Belyaev IN, Smolyaninov NP (1962) Zh Neorg Khim 7:1126
84. Yanovsky VK, Voronkova VI, Golub VN (1984) Kristallografiya 29:1193
85. Erman LYa, Galperin EL, Sobolev BP (1971) Zh Neorg Khim 16:490
86. Semenova HP (1989) Zh Neorg Khim 34:2336
87. Shebanov LA, Osipyan VG, Freidenfeld EZh (1982) Neorg Mater 18:305
88. Yanovsky VK, Voronkova VI, Rudenkova IA (1984) Kristallografiya 29:298
89. Yanovsky VK, Voronkova VI, Vodolazskaya IV (1990) Neorg Mater 26:1297
90. Koshelyaeva VG, Bush AA, Titov YuV, Venevtsev YuN (1988) Zh Neorg Khim 33:3143
91. Smolyaninov NP, Bochkareva OB, Marenich SS, Arbuzova AI (1971) Zh Neorg Khim 16:2299
92. Kargin YuF, Nelyapina NI, Skorikov VM (1983) Zh Neorg Khim 28:303
93. Yanovsky VK, Voronkova VI (1988) Kristallografiya 33:1278
94. Yanovsky VK, Voronkova VI (1986) Neorg Mater 22:2029
95. Korzunova LV, Osipyan VG, Shebanov LA, Freidenfeld EZh (1984) Neorg Mater 20:2074
96. Yanovsky VK, Voronkova VI, Leont'eva IN (1989) Neorg Mater 25:834
97. Neyman AYa, Kirpischikova TA (1996) Elektrokhimiya 32:511
98. Osipyan VG, Sittsa DA, Freidenfeld EZh (1982) Izv Sib Otd Akad Nauk SSSR Ser Khim 6:60
99. Kargin YuF, Skorikov VM, Kutvitsky VA, Zhereb VP (1977) Neorg Mater 13:132
100. Bordun OM (1998) Neorg Mater 34:1503
101. Skorikov VM, Speranskaya EI, Antonova SM (1969) In: Abstracts, Soviet meeting on thermography (in Russian). Nauka, Moscow, pp 103–105
102. Novikov GI, Butirin GM, Leonovich IB (1987) Vop Atom Nauki Tekhn Ser Atom-Vodorod Energ Tekhnol (1):42
103. Kazenas EK, Chizhikov DM, Tsvetkov YuV (1972) Dokl Akad Nauk SSSR 207:354
104. Kazenas EK, Chizhikov DM (1976) Pressure and composition of vapour over oxides of chemical elements (in Russian). Metallurgiya, Moscow
105. Yushina LD, Palguev SF (1964) Trudy Inst Elektrokhim (5):153
106. Kargin YuF, Kutvitsky VA, Skorikov VM (1977) Neorg Mater 13:128
107. Utkin VI, Roginskaya YuE, Voronkova VI, Yanovskii VK, Galyamov BSh, Venevtsev YuN (1980) Phys Status Solidi A 59:75
108. Shebanov LA, Osipyan VG, Freidenfeld EZh (1982) Phys Status Solidi A 71:61
109. Kovalevsky AV, Kharton VV, Naumovich EN (1999) Mater Lett 38:300
110. Katkov VF, Prushko IV, Kushnereva AK (1997) Neorg Mater 33:572
111. Chudinova NI, Lavrov AV, Tanaev IV (1972) Neorg Mater 8:1971
112. Zhereb LA (1983) PhD Thesis, Academy of Sciences of the USSR, Moscow
113. Volkov VV, Zhereb LA, Kargin YuF, Skorikov VM, Tananaev IV (1983) Zh Neorg Mater 28:1002
114. Smolyaninov NP, Belyaev IN (1963) Zh Neorg Khim 8:1219

115. Panchenko TV, Katkov VF, Kostyuk VKh (1983) Ukr Fiz Zh 28:1091
116. Burkov VI, Egorisheva AV, Kargin YuF, Mar'in AA (1998) Neorg Mater 34:962
117. Blinovskov YaN, Fotiev AA (1987) Zh Neorg Khim 32:254
118. Kargin YuF, Maryin AA, Skorikov VM (1982) Neorg Mater 18:1605
119. Bush AA, Stefanovich SYu, Titov YuV (1996) Zh Neorg Khim 41:1568
120. Kargin YuF, Voevodsky VYu (1997) Zh Neorg Khim 42:1547
121. Yudin AN, Kaplunnik LN, Mar'in AA (1989) Neorg Mater 25:313
122. Bush AA, Venevtsev YuI (1986) Zh Neorg Khim 31:1346
123. Berezovskaya YuM, Vasilyeva IA, Mayorova AF (1986) Zh Fiz Khim 60:1799
124. Shuvaeva ET, Fesenko EG (1980) Kristallografiya 25:406
125. Firsov AV, Bush AA, Mirkin AE, Venevtsev YuN (1985) Kristallografiya 30:932
126. Kargin YuF, Nelepina NI, Mar'in AA, Skorikov VM (1983) Neorg Mater 19:278
127. Smolevsky GA, Isupov VA, Golovschikova GI, Tutov AG (1976) Neorg Mater 12:297
128. Roth RS, Waring JL (1962) J Res Nat Bur Stand A 66:451
129. Verkerk MJ, Burggraaf AJ (1980) J Appl Electrochem 10:677
130. Mudretsova SN, Mayorova AF, Aleivi FH, Vasilyeva IA (1988) Vestn Moskov Univ Ser 2 29:463
131. Maydukova TP, Moskalenko TD, Grishaeva LA (1983) In: Materials for electronic technics (in Russian). Nauka, Moscow, pp 50–54
132. Borisov VN, Poplavko YuM, Avakyan PB, Osipyan VG (1988) Fiz Tverd Tela 30:1560
133. Osipyan VG, Savchenko LM, Elbakyan VL, Avakyan PB (1987) Neorg Mater 23:523
134. Mairesse G, Boivin JC, Lagrange G, Cocolios P (1994) Int Pat Appl CT WO 94/06545
135. Iharada T, Hammouche A, Fouletier J, Kleitz M, Boivin JC, Mairesse G (1991) Solid State Ionics 48:257
136. Yaremchenko AA, Kharton VV, Naumovich EN, Samokhval VV (1998) Solid State Ionics 111:227
137. Yaremchenko AA, Kharton VV, Mather GC, Naumovich EN, Marques FMB (1999) Bol Soc Esp Ceram Vidrio 38:635
138. Kargin YuF, Zhereb VP, Skorikov VM (1991) Zh Neorg Khim 36:2611
139. Speranskaya EI, Skorikov VM, Safronov GM, Mitkina GD (1968) Neorg Mater 4:1374
140. Kargin YuF (1995) Neorg Mater 31:88
141. Speranskaya EI, Skorikov VM (1967) Neorg Mater 3:345
142. Speranskaya EI, Rez IS, Kozlova LV, Skorikov VM, Slavov VI (1965) Neorg Mater 1:232
143. Belyaev IN, Smolyaninov NP, Kalnitsky NR (1963) Zh Neorg Khim 8:384
144. Speranskaya EI, Arshakuni AA (1964) Zh Neorg Khim 9:414
145. Shashkov Ayu, Efremov VM, Bush AA, Rannev NV, Venevtsev YuN, Trunov VK (1986) Zh Neorg Khim 31:1391
146. Skorikov VM, Kargin YuF, Nelyapina NI (1987) Zh Neorg Khim 32:1223
147. Kaplun AB, Meshalkin AB (1998) Neorg Mater 34:595
148. Koryagina TI, Kutvitsky VA, Skorikov VM, Kosov AV, Ustalova ON (1977) Zh Neorg Khim 22:773
149. Shimansky AF, Shvaiko-Shvaikovsky VE, Belenovich LN, Shpoo IYu, Glushkova VB, Novikov AI (1987) Zh Fiz Khim 61:3079
150. Dolgikh VA (1989) Zh Neorg Khim 34:2368
151. Prosichev II, Shaplygin IS, Komarov VP, Lazarev VB (1979) Zh Neorg Khim 24:2839
152. Popova TL, Kisel NG, Karlov VP, Bezrukov VI, Krivobok VI (1980) Zh Neorg Khim 25:1617
153. Prosichev II, Lazarev VB, Shaplygin IS (1981) Zh Neorg Mater 26:1877
154. Skorikov VM, Kargin YuF, Nelyapina NI (1988) Zh Neorg Khim 33:1354
155. Demina LA, Dolgikh VA, Popovkin BA, Novoselova AV (1979) Dokl Akad Nauk SSSR 244:94
156. Astafyev SA, Dolgikh VA, Popovkin BA (1989) Vestn Moskov Univ Ser 2 30:165
157. Shaplygin IS, Prosichev II, Lazarev VB (1981) Zh Neorg Khim 26:3338
158. Bondarev AD, Leonov EI, Mushinov IA, Nikitina IP, Orlov VM, Khokha LG (1985) Neorg Mater 21:1196
159. Safronov GM, Batog VN, Krasilov YuI, Pakhomov VI, Fedorov PM, Burkov VI, Skorikov VM (1970) Neorg Mater 6:284
160. Firsov AV, Bush AA, Mirkin AE, Venevtsev YuN (1985) Kristallografiya 30:927
161. Skorikov VM, Rza-zade PF, Kargin YuF, Djalaladdinov FF (1981) Zh Neorg Khim 26:1070
162. Shaplygin IS, Varlamov NV (1994) Neorg Mater 30:1478
163. Kargin YuF, Zhereb VP, Skorikov VM, Kosov AV, Kutvitsky VA, Nuriev EI (1977) Neorg Mater 13:135
164. Batog VN, Burkov VI, Kizel VA, Madiy VA, Safronov GM, Skorikov VM (1969) Kristallografiya 14:928
165. Egorisheva AV, Burkov VI, Kargin YuF, Volkov VV (1995) Neorg Mater 31:1087
166. Kargin YuF, Khomich AV, Perov PI, Skorikov VM (1985) Neorg Mater 21:1973
167. Zhereb VP, Kargin YuF, Skorikov VM (1978) Neorg Mater 14:2029
168. Kargin YuF, Maryin AA, Vasilyev LYa, Chmirev VI, Skorikov VM (1981) Neorg Mater 17:1428
169. Tarasova LS, Kosov AV (1982) Neorg Mater 18:1615
170. Tananaev IV, Skorikov VM, Kutvitsky VA, Voskresenskaya EN (1981) Neorg Mater 17:663
171. Kutvitsky VA, Skorikov VM, Voskresenskaya EN, Grekhova TI, Shadeev NI (1979) Neorg Mater 15:1844
172. Kalinkin AN, Skorikov VM, Soldatov AA (1992) Neorg Mater 28:558
173. Zakharov IS, Skorikov VM, Petukhov PA, Kargin YuF, Volkov VV (1985) Fiz Tverd Tela 27:597
174. Ivanov VV (1983) Interpretation for IR spectra of $6Bi_2O_3{\cdot}CeO_2$, $6Bi_2O_3{\cdot}SiO_2$, and $6Bi_2O_3{\cdot}ZnO_2$ compounds (in Russian). VINITI, Zernograd
175. Kravchenko EA, Fam Suan Hay, Kargin YuF (1997) Neorg Mater 33:1001
176. Smirnov VI, Yukhin YuM (1997) Zh Neorg Khim 42:1450
177. Kosov AV, Endrzhevskaya VYu (1986) Neorg Mater 22:1701
178. Kaminsky AA, Sarkisov SE, Mayer AA, Lomonov VA, Asafov DV, Zakaznov PN (1983) Neorg Mater 19:1148
179. Zhereb VP (1980) PhD Thesis, Academy of Sciences of the USSR, Moscow
180. Kargin YuF, Egorisheva AV (1998) Neorg Mater 34:859
181. Zargareva MI, Shuster NS (1993) Neorg Mater 29:535
182. Speranskaya EI, Skorikov VM, Safronov TM, Gaydukov EN (1970) Neorg Mater 6:1364
183. Surnina VS, Litvin BN (1970) Kristallografiya 15:604
184. Safronov GM, Speranskaya EI, Batog VN, Mitkina GD, Fedorov PM, Gubina TF (1971) Zh Neorg Khim 16:526
185. Djalaladdinov FF (1984) PhD Thesis, Academy of Sciences of the USSR, Moscow
186. Romanov VP, Varfolomeev MB (1976) Zh Neorg Khim 21:2635
187. Yaremchenko AA, Kharton VV, Viscup AP, Naumovich EN, Vecher AA (1997) Vestn Belarus Univ Ser 2 (3):15
188. Levin EM, Roth RS (1964) J Res Nat Bur Stand A 68:197
189. Bronin DI, Kuzin BL, Nafe H, Aldinger F (1999) J Electrochem Soc 146:2034
190. Bronin DI, Kuzin BL, Nafe H, Aldinger F (1999) Solid State Ionics 120:13
191. Zhitomirsky ID, Fedotov SV, Skorokhodov NE, Bush AA, Mar'in AA, Venevtsev YuN (1983) Zh Neorg Knim 28:1006
192. Reznitsky LA (1979) DSc Thesis, Moscow State University, Moscow
193. Belkova TB, Krapivina KG, Neyman AYa (1998) In: Burmakin EI, Balakireva VB (eds) Abstracts, XI conference on

physical chemistry and electrochemistry of melted and solid electrolytes, vol 2 (in Russian). Russian Academy of Sciences, Ural Dept., Ekaterinburg, p 83
194. Tutov AG, Milnikova IE, Parfenova VA, Bokov SA, Kizhaev SA (1964) Fiz Tverd Tela 6:1240
195. Speranskaya EI, Skorikov VM, Rode EYa, Terekhova VA (1965) Izv Akad Nauk SSSR Ser Khim (5):905
196. Speranskaya EI, Skorikov VM (1967) Neorg Mater 3:341
197. Zakharov AA, Shaplygin IS, Shubrt AT (1982) Izv Sib Otd Akad Nauk SSSR Ser Khim 6:69
198. Tomashpolsky YuYa, Skorikov VM, Venevtsev YuN, Speranskaya EI (1966) Neorg Mater 2:707
199. Gorashenko NG, Kuchuk ZhS, Mayer AA, Balashov VA (1985) In: Abstracts, VI Soviet conference on crystal growth (in Russian). Academy of Sciences of the Armenian SSR, Erevan, pp 84–85
200. Kharton VV (1993) PhD Thesis, Belarus State University, Minsk
201. Roginskaya YuE, Venevtsev YuN, Fedulov SA, Zhdanov GS (1963) Kristallografiya 8:610
202. Viskov AS, Venevtsev YuN, Petrov VM, Volkov AF (1968) Neorg Mater 4:88
203. Fedulov SA (1962) PhD Thesis, Academy of Sciences of the USSR, Moscow
204. Dugar-Zhabon KD (1972) Neorg Mater 8:505
205. Boray-Brvar A, Trontee M, Kolar D (1979) J Less Common Met 68:7
206. Kharton VV, Naumovich EN, Zhuk PP (1992) In: Abstracts, XI meeting on kinetics and mechanism of chemical reactions in solids (in Russian). Russian Academy of Sciences, Chernogolovka, pp 301–302
207. Kharton VV, Zhuk PP, Naumovich EN, Zinkevich MV, Vecher AA (1991) USSR Pat 1763421
208. Fedulov SA, Venevtsev YuN, Zhdanov GS, Smazhevskaya EP (1964) Kristallografiya 9:516
209. Rakov DN, Murashov VA, Bush AA, Venevtsev YuN (1988) Kristallografiya 33:445
210. Shuk P, Jakobs S, Möbius HH (1985) Z Anorg Allg Chem 524:144
211. Shuk PP, Vecher AA, Samochval VV (1985) Thermochim Acta 93:461
212. Shuk P, Jacobs S, Mobius HH (1980) In: Hauptjahrestag Chem Ges DDR (in German). Academy of Sciences of the DDR, Karl-Max-Stadt, p 100
213. Möbius HH, Zhuk PP, Jakobs S, Hartung R, Guth U, Sandov H, Vecher AA (1990) Elektrokhimiya 26:1388
214. Zhuk PP, Vecher AA, Hartung R, Samokhval VV, Möbius HH (1986) Vesti Akad Nauk BSSR Ser Khim (6):44
215. Zhuk PP, Vecher AA, Möbius HH, Jakobs S (1987) Vestn Belarus Univ Ser 2 (2):14
216. Viting LM, Golubeva NN, Gorbovskaya GP (1967) Vestn Mosk Univ Ser 2 22:89
217. Slobodin BV, Vasilyev VG, Soldatova EE (1997) Zh Neorg Khim 42:1740
218. Slobodin BV, Vasilyev VG, Soldatova EE (1998) In: Burmakin EI, Balakireva VB (eds) Abstracts, XI conference on physical chemistry and electrochemistry of melted and solid electrolytes, vol 2 (in Russian). Russian Academy of Sciences, Ural Dept., Ekaterinburg, p 93
219. Slobodin BV, Fotiev AA (1994) Zh Neorg Khim 39:1198
220. Zinkevich MV, Prodan SA, Zonov YuG, Vashuk VV (1995) Neorg Mater 31:142
221. Zinkevich MV, Vashuk VV (1994) Elektrokhimiya 30:1172
222. Moiseev G, Ziablikova N, Jzukovski V, Zaitseva S (1996) Thermochim Acta 283:191
223. Klinkova LA, Nikolaychik VI, Zorina LV, Barkovsky NV, Fedotov VK, Zverkov SA (1996) Zh Neorg Khim 41:709
224. Shevchuk AV, Skorikov VM, Kargin YuF, Konstantinov VV (1985) Zh Neorg Khim 30:1519
225. Klinkova LA, Nikolaychik VI, Barkovsky NV, Fedotov VK (1997) Zh Neorg Khim 42:1550
226. Klinkova LA, Nikolaychik VI, Barkovsky NV, Fedotov VK (1997) Zh Neorg Khim 42:905
227. Poluyan AF, Babushkin OS, Shuk PP (1986) In: 37th meeting International Society of Electrochemistry, ext abstr, vol 3. VINITI, Lubertsy, pp 76–78
228. Viting LM, Gorbovskaya GP (1967) Vestn Mosk Univ Ser 2 22:92
229. Yaremchenko AA, Kharton VV, Viskup AP, Naumovich EN, Samokhval VV (1998) Mater Res Bull 33:1027
230. Yaremchenko AA, Kharton VV, Kovalevsky AV, Lapchuk NM, Naumovich EN (2000) Mater Chem Phys 63:240
231. Klinkova LA (1994) Sverkhprovodimost: Fiz Khim Tekhn 7:418
232. Klinkova LA, Filatova MV, Barkovsky NV, Batova DE (1991) Zh Neorg Khim 36:547
233. Biefeld RM, White SS (1981) J Am Ceram Soc 64:182
234. Sammes NM, Tompsett G, Gartner AM (1995) J Mater Sci 30:4299
235. Kakhan BG, Lazarev VB, Shaplygin IS (1979) Zh Neorg Khim 24:1663
236. Kargin YuF, Skorikov VM (1989) Zh Neorg Khim 34:2713
237. Lazarev VB, Shaplygin IS (1974) Zh Neorg Khim 19:2388
238. Kakhan BG, Lazarev VL, Shaplygin IS, Ellert OG (1981) Zh Neorg Khim 26:232
239. Klyndyuk AI, Petrov GS, Bashkirov LA, Akimov AI, Poluyan AF (1999) Zh Neorg Khim 44:5
240. Belousov VV, Konev VV, Roslik AK (1990) Sverkhprovodimost: Fiz Khim Tekhn 3:1890
241. Kharton VV, Nikolaev AV, Naumovich EN, Vecher AA (1995) Solid State Ionics 81:201
242. Tikhonovich VN, Bochkov DM, Kharton VV, Naumovich EN, Viscup AP (1998) Mater Res Bull 33:89
243. Konev BN, Belousov VV, Nadolsky AL (1987) In: Abstracts, IX Soviet conference on physical chemistry and electrochemistry of ionic melts and solid electrolytes, vol 3 (in Russian). Academy of Sciences of the USSR, Ural Dept., Sverdlovsk, p 75
244. Nedilko SA, Zyryanova NP, Panchenko GV (1986) Ukr Khim Zh 52:356
245. Slobodin BV, Ostapenko IA, Fotiev AA (1992) Zh Neorg Khim 37:438
246. Poluyan AF, Babushkin OS, Vecher AA (1986) In: 37th meeting International Society of Electrochemistry, ext abstr, vol 3. VINITI, Lubertsy, pp 207–209
247. Safronov GM, Batog VN, Stepanyuk TV, Fedorov PM (1971) Zh Neorg Khim 16:863
248. Shimansky AF, Koryagina TI, Kirik SD, Kutvitsky VA, Belenovich LI (1991) Neorg Mater 27:1095
249. Kirik SD, Kutvitsky VA, Koryagina TI (1985) Zh Strukt Khim 26:90
250. Kutvitsky VA, Kosov AV, Skorikov VM, Koryagina TI (1975) Neorg Mater 11:2190
251. Kirik SD, Kutvitsky VA, Koryagina TI, Shimansky AF (1989) Zh Strukt Khim 30:111
252. Schenev AV, Skorikov VM, Kargin YuF (1988) Zh Neorg Khim 33:721
253. Kirik SD, Shimanskiy AF, Koryagina TI (1999) Solid State Ionics 122:249
254. Kirik SD, Tzurgan LS, Pervyshina GG, Koryagina TI, Kutvitsky VA (1992) Zh Strukt Khim 30:1410
255. Kutvitsky VA, Kosov AV, Skorikov VM, Zhereb VN, Kargin YuF (1976) Zh Neorg Khim 21:529
256. Mechev VV, Andreev AA, Melekh BG, Kirik SD, Filin YuI, Shimansky AF, Koryagina TI, Ustalova OI (1985) Zh Prikl Khim 58:478
257. Kargin YuF, Kosov AV, Kutvitsky VA, Skorikov VM, Kiselev VB (1975) Neorg Mater 11:1826
258. Valeev HS, Baklanov EG (1971) Neorg Mater 7:1463
259. Bochkov DM, Kharton VV, Kovalevsky AV, Viskup AP, Naumovich EN (1999) Solid State Ionics 120:281
260. Kharton VV, Viskup AP, Naumovich EN, Marques FMB (1999) J Mater Chem 9:2623

261. Tikhonovich VN, Kharton VV, Naumovich EN, Savitsky AA (1998) Solid State Ionics 106:197
262. Nikolaev AV, Kharton VV, Naumovich EN, Vecher AA (1994) In: Bossel U (ed) Proc 1st Europ SOFC Forum, vol 1. Lucerne, pp 415–424
263. Naumovich EN, Kharton VV, Vecher AA (1998) In: Sviridov VV (ed) Chemical problems of developing new materials and technologies (in Russian). Belarus State University, Minsk, pp 431–450
264. Naumovich EN, Skilkov SA, Kharton VV, Vecher AA (1994) Solid State Phenom 39–40:243
265. Poluyan AF, Voropaev AG, Dubok VA, Markov NI, Vecher AA (1988) Vesti Akad Nauk BSSR Ser Khim (5):38
266. Poluyan AF, Zhuk PP, Vecher AA, Samokhval VV (1986) Neorg Mater 22:1691
267. Polujan AF, Shuk PP, Vecher AA (1985) In: Proc int symp on systems with fast ionic transport. Smolevice, pp 137–141
268. Poluyan AF, Samokhval VV, Savitsky AA (1985) Thermochim Acta 93:465
269. Kharton VV, Zhuk PP, Naumovich EN, Vecher AA, Tonoyan AA (1991) USSR Pat 1794931
270. Samokhval VV (2000) DSc Thesis, Belarus State University, Minsk
271. Zinkevich MV, Vashook VV, Zonov YuG, Prodan SA, Olshevskaya OP (1994) Vesti Akad Nauk Belarusi Ser Khim (3):66
272. Vashook VV, Olshevskaya OP, Strukova OV, Nesterenko NB (1997) Neorg Mater 33:472
273. Vashook VV, Olshevskaya OP, Pitlev SI, Vilkotskaya EF, Zinkevich MV (1998) Neorg Mater 34:67
274. Vashook VV, Olshevskaya OP, Zonov YuG, Strukova OV (1998) Vesti Akad Nauk Belarusi Ser Khim (1):5
275. Zinkevich MV, Prodan SA, Zonov YuG, Vashook VV (1998) J Solid State Chem 136:1
276. Virkar AV, Fung KZ (1993) US Pat 5183801
277. Bogdanovich NM, Vlasov AN, Neuimin AD, Kuzmin BV (1998) In: Burmakin EI, Balakireva VB (eds) Abstracts, XI conference on physical chemistry and electrochemistry of melted and solid electrolytes, vol 2 (in Russian). Russian Academy of Sciences, Ural Dept., Ekaterinburg, pp 16–17
278. Kharton VV, Naumovich EN, Zhuk PP, Demin AK, Nikolaev AV (1992) Russ J Electrochem 28:1376
279. Kharton VV, Naumovich EN, Nikolaev AV, Astashko VV, Vecher AA (1993) Russ J Electrochem 29:1039
280. Voskresenskaya EI (1983) PhD Thesis, Academy of Sciences of the USSR, Moscow
281. Kharton VV, Zhuk PP, Demin AK, Nikolaev AV, Tonoyan AA, Vecher AA (1992) In: Perfilyev MV (ed) Ionics of solid state (in Russian). Nauka, Ekaterinburg, pp 3–13
282. Zhuk PP, Zinkevich MV, Kharton VV, Vecher AA (1991) Vestn Belarus Univ Ser 2 (2):18
283. Kharton VV, Naumovich EN, Nikolaev AV (1996) J Membr Sci 111:149
284. Naumovich EN, Zhuk PP, Vecher AA, Kurumchin EH (1993) In: Perfilyev MV (ed) Ionics of the solid state (in Russian). Nauka, Ekaterinburg, pp 27–38
285. Gorelov GP, Kurumchin EKh, Ishuk VP (1988) Zh Fiz Khim 62:815
286. Kurumchin EH (1990) In: Perfilyev MV (ed) Electrode reactions in solid electrolytes (in Russian). Academy of Sciences of the USSR, Ural Dept., Sverdlovsk, pp 63–79
287. Kurumchin EH, Vdovin GK, Gorelov GP, Zhuk PP, Naumovich EN (1993) In: Perfilyev MV (ed) Ionics of the solid state (in Russian). Nauka, Ekaterinburg, pp 39–45
288. Kurumchin EH, Perfilyev MV (1990) Solid State Ionics 42:129
289. Kurumchin EH (1997) DSc Thesis, Russian Academy of Sciences, Ekaterinburg
290. Kurumchin EH (1998) Ionics 4:390
291. Popovsky VV, Boreskov GK, Muzykantov VS (1969) Kinet Katal 10:786
292. Kurumchin EKh, Ischuk VP, Gorelov GP (1986) In: High-temperature electrochemistry: electrolytes, kinetics (in Russian). Academy of Sciences of the USSR, Ural Dept., Sverdlovsk, pp 87–96
293. Kurumchin EH, Vdovin GK, Fotiev AA, Leonidova ON (1994) Solid State Ionics 70–71:77
294. Kurumchin EKh, Vdovin GK, Fotiev AA (1992) Sverkhprovodimost: Fiz Khim Tekhn 5:2360
295. Muzykantov VS, Popovsky VV, Boreskov GK (1964) Kinet Katal 5:624
296. Muzykantov VS, Panov GI, Boreskov GK (1973) Kinet Katal 24:948
297. Naumovich EN, Shuk PP, Vecher AA (1991) Mater Sci Forum 76:65
298. Kharton VV, Naumovich EN, Nikolaev AV, Vecher AA (1993) Vesti Akad Nauk Belarusi Ser Khim (3):53
299. Lobovikova NA, Perfilyev MV (1988) In: Perfilyev MV (ed) Electrode processes in solid-electrolyte systems (in Russian). Academy of Sciences of the USSR, Ural Dept., Sverdlovsk, pp 67–84
300. Lobovikova NA (1985) PhD Thesis, Academy of Sciences of the USSR, Ural Dept., Sverdlovsk
301. Kharton VV, Nikolaev AV, Naumovich EN, Samokhval VV (1994) Inorg Mater 30:492
302. Kharton VV, Astashko VV, Zhuk PP, Demin AK, Nikolaev AV, Gilevich MP, Vecher AA (1992) Vesti Akad Nauk Belarusi Ser Khim (1):47
303. Naumovich EN, Zhuk PP, Vecher AA, Tikhonova LA, Tonoyan AA (1990) USSR Pat 1684652
304. Gavrilov AG, Neuimin AD, Yushina LD (1998) In: Burmakin EI, Balakireva VB (eds) Abstracts, XI conference on physical chemistry and electrochemistry of melted and solid electrolytes, vol 2 (in Russian). Russian Academy of Sciences, Ural Dept., Ekaterinburg, p 156
305. Naumovich EN, Kharton VV, Shuk PP, Vecher AA (1991) In: Abstracts, Soviet conference on current state of analytical instrument production in the field of gas medium analysis and radiospectroscopy (in Russian). Analitpribor, Smolensk, p 239
306. Kharton VV, Zhuk PP, Demin AK, Nikolaev AV, Tonoyan AA, Vecher AA (1992) Inorg Mater 28:1406